SYSTEM MANUALS

of BASEMENT

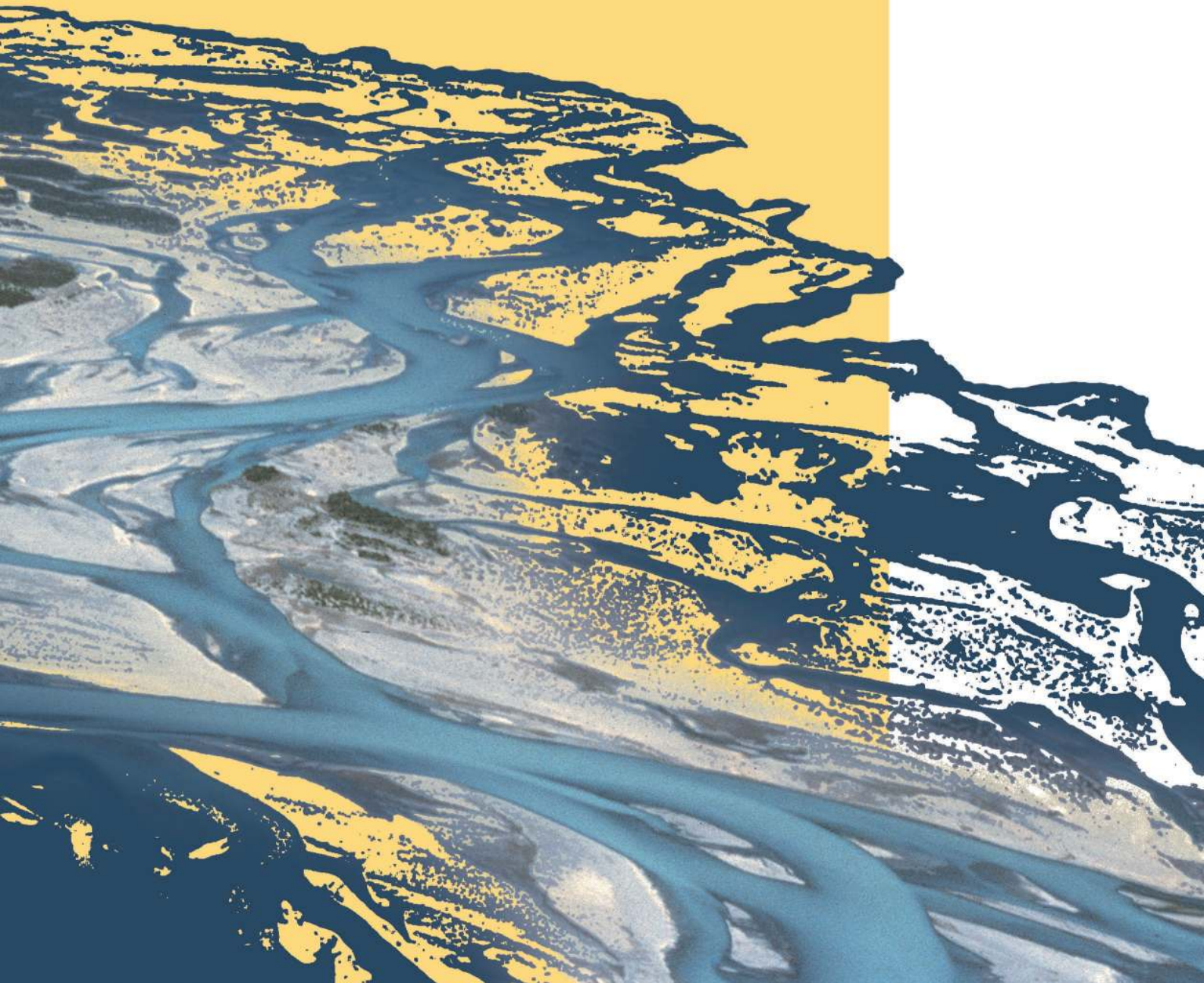

TC

TEST CASES

of BASEMENT

Contents

Preamble

VERSION 2.8.1

November, 2020

Credits

Project Team

Software Development, Documentation and Test (alphabetical)

M. Bürgler, MSc. ETH Environmental Eng.
F. Caponi, MSc. Environmental Eng.
Dr. D. Conde, MSc. Civil Eng.
E. Gerke, MSc. ETH Civil Eng.
S. Kammerer, MSc. ETH Environmental Eng.
Dr.techn. M. Weberndorfer, MSc.

Scientific Board

Prof. Dr. R. Boes, Director VAW, Member of Project Board
Dr. A. Siviglia, MSc, Scientific Adivisor
Dr. D. Vanzo, MSc. Environmental Eng., Scientific Adivisor
Dr. D. Vetsch, Dipl. Ing. ETH, Project Director

Former Project Members

See https://www.basement.ethz.ch/people

Cover Page Art Design

W. Thürig

Commissioned and co-financed by

Swiss Federal Office for the Environment (FOEN)

Contact

website: http://www.basement.ethz.ch
user forum: http://people.ee.ethz.ch/~basement/forum

Citation Advice

For System Manuals:

Vetsch D., Siviglia A., Bürgler M., Caponi F., Ehrbar D., Facchini M., Faeh R., Farshi D., Gerber M., Gerke E., Kammerer S., Koch A., Mueller R., Peter S., Rousselot P., Vanzo D., Veprek R., Volz C., Vonwiller L., Weberndorfer M. 2020. System Manuals of BASEMENT, Version 2.8.1 Laboratory of Hydraulics, Glaciology and Hydrology (VAW). ETH Zurich. Available from http://www.basement.ethz.ch. [date of access].

For Website:

BASEMENT – Basic Simulation Environment for Computation of Environmental Flow and Natural Hazard Simulation, 2020. http://www.basement.ethz.ch

For Software:

BASEMENT – Basic Simulation Environment for Computation of Environmental Flow and Natural Hazard Simulation. Version 2.8.1 © ETH Zurich, VAW, 2006-2020.

License

BASEMENT SOFTWARE LICENSE

between

ETH

Rämistrasse 101

8092 Zürich

Represented by Prof. Dr. Robert Boes

VAW

(Licensor)

and

Licensee

1. Definition of the Software

The Software system BASEMENT is composed of the executable (binary) file BASEMENT and its documentation files (System Manuals), together herein after referred to as "Software". Not included is the source code.

Its purpose is the simulation of water flow, sediment and pollutant transport and according interaction in consideration of movable boundaries and morphological changes.

2. License of ETH

ETH hereby grants a single, non-exclusive, world-wide, royalty-free license to use Software to the licensee subject to all the terms and conditions of this Agreement.

3. The scope of the license

a. Use

The licensee may use the Software:

- according to the intended purpose of the Software as defined in provision 1
- by the licensee and his employees
- for commercial and non-commercial purposes

The generation of essential temporary backups is allowed.

b. Reproduction / Modification

Neither reproduction (other than plain backup copies) nor modification is permitted with the following exceptions:

Decoding according to article 21 URG [Bundesgesetz über das Urheberrecht, SR 231.1)

If the licensee intends to access the program with other interoperative programs according to article 21 URG, he is to contact licensor explaining his requirement.
If the licensor neither provides according support for the interoperative programs nor makes

the necessary source code available within 30 days, licensee is entitled, after reminding the licensor once, to obtain the information for the above mentioned intentions by source code generation through decompilation.

c. Adaptation

On his own risk, the licensee has the right to parameterize the Software or to access the Software with interoperable programs within the aforementioned scope of the licence.

d. Distribution of Software to sub licensees

Licensee may transfer this Software in its original form to sub licensees. Sub licensees have to agree to all terms and conditions of this Agreement. It is prohibited to impose any further restrictions on the sub licensees' exercise of the rights granted herein.

No fees may be charged for use, reproduction, modification or distribution of this Software, neither in unmodified nor incorporated forms, with the exception of a fee for the physical act of transferring a copy or for an additional warranty protection.

4. Obligations of licensee

a. Copyright Notice

Software as well as interactively generated output must conspicuously and appropriately quote the following copyright notices:

Copyright by ETH Zurich / Laboratory of Hydraulics, Glaciology and Hydrology (VAW), 2006-2018

5. Intellectual property and other rights

The licensee obtains all rights granted in this Agreement and retains all rights to results from the use of the Software.

Ownership, intellectual property rights and all other rights in and to the Software shall remain with ETH (licensor).

6. Installation, maintenance, support, upgrades or new releases

a. Installation

The licensee may download the Software from the web page http://www.basement.ethz.ch or access it from the distributed CD.

b. Maintenance, support, upgrades or new releases

ETH doesn't have any obligation of maintenance, support, upgrades or new releases, and disclaims all costs associated with service, repair or correction.

7. Warranty

ETH does not make any warranty concerning the:

- warranty of merchantability, satisfactory quality and fitness for a particular purpose
- warranty of accuracy of results, of the quality and performance of the Software;
- warranty of noninfringement of intellectual property rights of third parties.

8. Liability

ETH disclaims all liabilities. ETH shall not have any liability for any direct or indirect damage except for the provisions of the applicable law (article 100 OR [Schweizerisches Obligationenrecht]).

9. Termination

This Agreement may be terminated by ETH at any time, in case of a fundamental breach of the provisions of this Agreement by the licensee.

10. No transfer of rights and duties

Rights and duties derived from this Agreement shall not be transferred to third parties without the written acceptance of the licensor. In particular, the Software cannot be sold, licensed or rented out to third parties by the licensee.

11. No implied grant of rights

The parties shall not infer from this Agreement any other rights, including licenses, than those that are explicitly stated herein.

12. Severability

If any provisions of this Agreement will become invalid or unenforceable, such invalidity or enforceability shall not affect the other provisions of Agreement. These shall remain in full force and effect, provided that the basic intent of the parties is preserved. The parties will in good faith negotiate substitute provisions to replace invalid or unenforceable provisions which reflect the original intentions of the parties as closely as possible and maintain the economic balance between the parties.

13. Applicable law

This Agreement as well as any and all matters arising out of it shall exclusively be governed by and interpreted in accordance with the laws of , excluding its principles of conflict of laws.

14. Jurisdiction

If any dispute, controversy or difference arises between the Parties in connection with this Agreement, the parties shall first attempt to settle it amicably.
Should settlement not be achieved, the Courts of Zurich-City shall have exclusive jurisdiction.
This provision shall only apply to licenses between ETH and foreign licensees

By using this software you indicate your acceptance.

(License version: 2018-05-31)

THIRD PARTY SOFTWARE

BASEMENT uses third party software. For instance, the BASEMENT executable directly links the following external libraries:

- CGNS
- HDF5
- Qt5 (non-cluster version only)
- Qwt (non-cluster version only)
- Shapelib
- TecIO
- VTK (non-cluster version only)

The libraries (and their dependencies) are included in the BASEMENT distribution if they are not provided by the operating system.

Please refer to `ThirdPartySoftwareLicenses.txt` in the distribution and/or the operating system documentation for the third party software licenses and copyright notices. The external libraries for Windows 10 have been built using `vcpkg` version 2020.07 (`HDF5` was compiled without `szip`).

1

Hydrodynamics

1.1 Introduction

The test catalogue is intended for the validation of the program. The catalogue consists of different test cases, their geometric and hydraulic fundamentals and the reference data for the comparison with the computed results. The test cases are built up on each other going from easy to more and more complex problems. The hydraulic solver is validated against analytical and experimental solutions using the test cases in Section 1.2. Common test cases are suitable for both, 1-D and 2-D simulations. Specific test cases are intended for either 1-D or 2-D simulations.

1.2 Common Test Cases

1.2.1 H_1: Dam break in a closed channel

1.2.1.1 Intention

The simplest test case check verifies the conservation property of the fluid phase and whether a stable condition can be reached for all control volumes after a finite time. Additionally, wet and dry problematic is tested.

1.2.1.2 Description

Consider a rectangular flume without sediment. The basin is initially filled in the half length with a certain water depth leaving the other side dry. After starting the simulation, the water flows in the other half of the system until it reaches a quiescent state (velocity = 0, half of initial water surface elevation (WSE) everywhere).

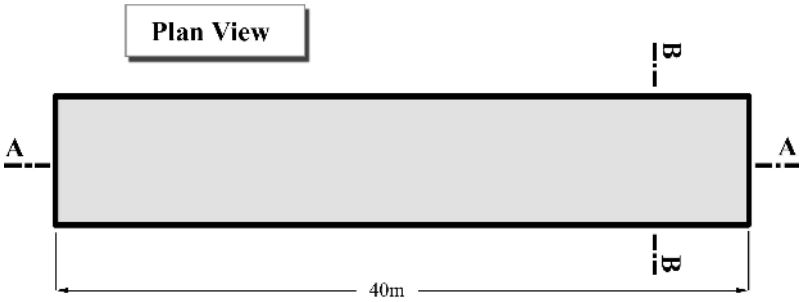

Figure 1.1 *H_1: Dam break in a closed channel, plan view*

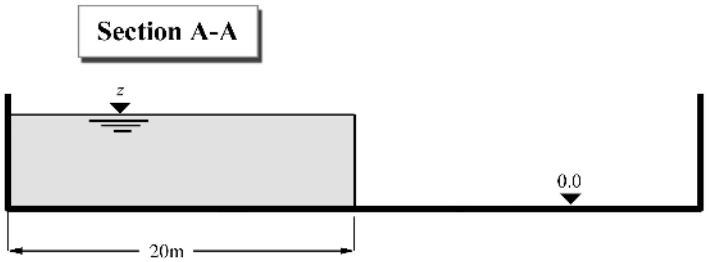

Figure 1.2 *H_1: Dam break in a closed channel, section A-A*

1.2.1.3 Geometry and Initial Conditions

Initial Condition: water at rest (all velocities zero), the water surface elevation is the same on the half of channel. This test uses a WSE of $z_S = 5.0$ m.

1.2.1.4 Boundary Conditions

No inflow and outflow. All of the boundaries are considered as a wall.

Friction: Manning's factor $n = 0.010$

1.2.2 H_2: One dimensional dam break on planar bed

1.2.2.1 Intention

This test case is similar to the previous one but this one compares the WSE a short time after release of the dam with an analytical solution for this frictionless problem. It is based on the verification of a 1-D transcritical flow model in channels by Tseng (1999).

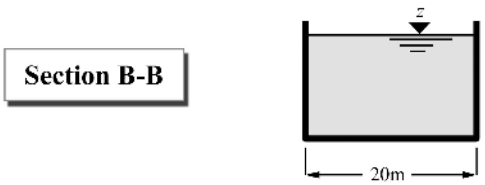

Figure 1.3 *H_1: Dam break in a closed channel, section B-B*

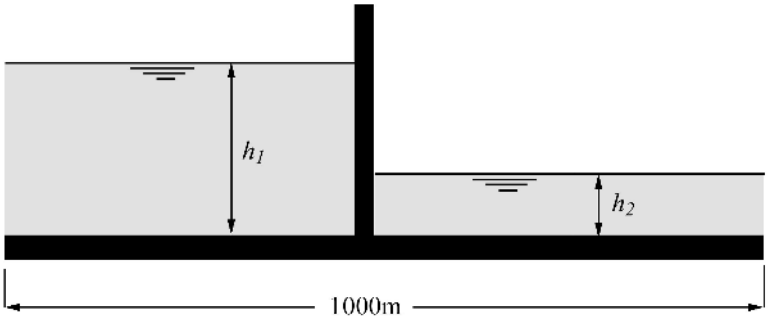

Figure 1.4 *H_2: One dimensional dam break on planar bed*

1.2.2.2 Description

A planar, frictionless rectangular flume has initially a dam in the middle. On one side, the water level is h_2 , on the other side, the water level is at h_1. At the beginning, the dam is removed and a wave is propagating towards the shallow water. The shape of the wave depends on the fraction of the water depths (h_2/h_1) and can be compared to an analytical, exact solution.

1.2.2.3 Geometry and Initial Conditions

Two cases are considered:

- h_2/h_1= 0.001 ; h_1 = 10.0 m (this avoids problems with wet/dry areas)
- h_2/h_1= 0.000 ; h_1 = 10.0 m (downstream is initially dry)

The dam is exactly in the middle of the channel.

Since it is a one dimensional problem, it should not depend on the width of the model, which can be chosen arbitrary.

1.2.2.4 Boundary Conditions

All cases are frictionless, Manning factor n=0.

1.2.3 H_3: One dimensional dam break on sloped bed

1.2.3.1 Intention

Different from the previous cases, this problem uses a sloped bed with friction. The aim is to reproduce an accurate wave front in time. It is based on the verification of a 1-D transcritical flow model in channels by Tseng (1999).

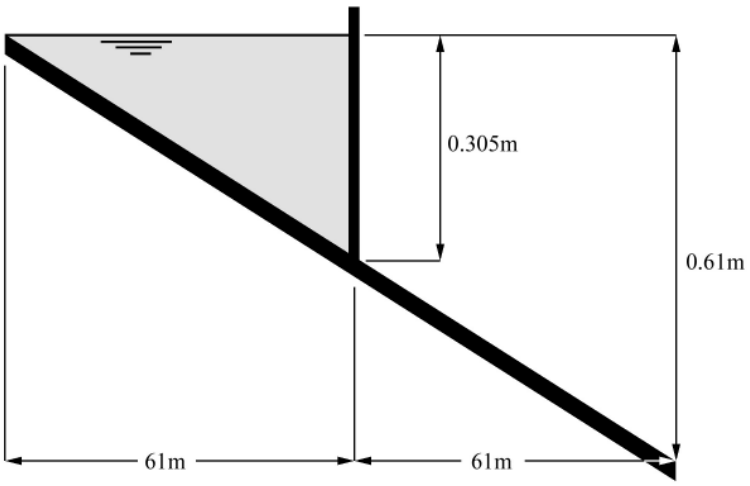

Figure 1.5 *H_3: One dimensional dam break on sloped bed*

1.2.3.2 Description

In the middle of a slightly sloped flume, an initial dam is removed at time zero (see Figure 1.5). The wave propagates downwards. Comparison data comes from an experimental work. Friction is accounted for with a Manning roughness factor estimated from the experiment.

1.2.3.3 Geometry and Initial Conditions

Length of flume:	122 m
Width of flume:	1.22 m
Slope:	0.61 m/122 m
Initial water level:	0.035 m (at the dam location)

1.2.3.4 Boundary Conditions

Manning friction factor: 0.009

No inflow/outflow. Boundaries are considered as walls.

1.2.4 H_4 : Parallel execution

1.2.4.1 Intention

To test the parallel performance of hydraulic simulations on a multi-core shared memory computer a test case is set up. The aim is to demonstrate the increase in performance (the speedup) when running BASEMENT in parallel with an increasing number of cores.

1.2.4.2 Description

A hydraulic simulation is repeated with varying number of threads on a multi-core shared memory system. The simulation times are measured and compared to the sequential

execution time in order to evaluate the speedups.

1.2.4.3 Geometry, initial conditions and boundary conditions

A simple rectangular channel with constant slope is considered. The channel is discretized with a large number of cross sections (2000) in BASEchain and a large number of elements (16000) in BASEplane. There is an inflow located at the upper boundary of the channel and an outflow at the lower boundary. The inflowing discharge is constant over the time and steady state conditions within the channel are reached.

Large sized scenarios and evenly distributed work loads (steady state conditions) are set up in order to check for the full potential of the parallel implementation.

1.2.5 H_5: Controlled Boundary Condition

1.2.5.1 Intention

To verify and test the correct action of a PID-controller, steering a boundary condition to keep the water level at a certain cross section or element on the predefined level.

1.2.5.2 Description

The calculation includes a simple channel ending with a weir. In 2-D, two parallel channels are given. One channel is terminated with a weir, the other with a gate. The weir height and gate level is controlled during the simulation by the PID controller and is automatically updated to maintain the predefined water level.

For the 1-D simulation, the discharge in steady state is 100 m^3/s. Over 5000 seconds it is increased up to 150 m^3/s. The water level is fixed at QP_A18 to 112.6 m. The calculation also includes a feed forward component, directly translating the deviation of the inflow from steady state into an adaption of the weir height.

In 2-D, the discharge is increased from 300 m^3/s to 450 m^3/s and then lowered to 180 m^3/s before it is again set to 300 m^3/s. For the 2-D simulation, the target level is not constant, but dependent on the current inflow, which is measured upstream.

Inflow (m^3/s)	Water level (m)
150	503.0
300	503.2
450	503.4

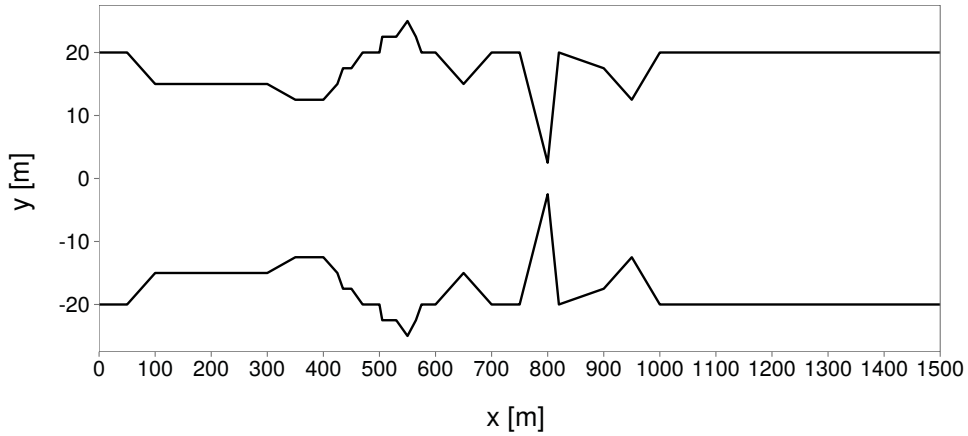

Figure 1.6 *H_BC_1: Top view: cross-sections*

1.3 BASEchain Specific Test Cases

1.3.1 H_BC_1: Fluid at rest in a closed channel with strongly varying geometry

1.3.1.1 Intention

This test case checks for the conservation of momentum. Numerical artefacts (mostly due to geometrical reasons) could generate impulse waves although there is no acting force.

1.3.1.2 Description

The computational area consists of a rectangular channel with varying bed topology and different cross-sections. The fluid is initially at rest with a constant water surface elevation and there is no acting force. There should be no changes of the WSE in time.

1.3.1.3 Geometry and Initial Conditions

The cross sections and bed topology were chosen as in Figure 1.6 and Figure 1.7. Notice the strong variations within the geometry. The water surface elevation is set to $z_S = 12$ m.

1.3.1.4 Boundary Conditions

All boundaries are considered as walls. There is no friction acting.

1.3.2 H_BC_2: bed load simulation with implicit hydraulic solution

1.3.2.1 Intention

The aim of this test case is to verify if the use of the implicit computation mode leads to the expected gain of computational time for a long sediment transport simulation.

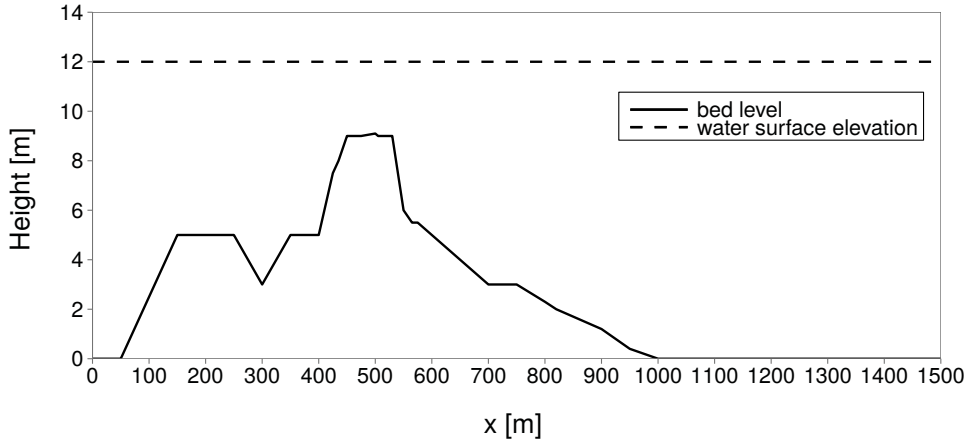

Figure 1.7 *H_BC_1: Bed topography and water surface elevation*

1.3.2.2 Description

The test case simulates a section of the river Thur near Altikon. At this place, there is a widening of which the morphological evolution should be evaluated.

1.3.2.3 Geometry and general data

The model is composed by 55 irregular cross sections, the mean grain size is 2.5 cm and the length of the transport generating hydrograph is 338 hours. The given time steps for the implicit simulation are 60, 120 and 180 seconds. The Program is allowed to reduce the time step if necessary, but this leads to time loss. The precisions of the results for which the iteration is interrupted are 0.1 m^2 for the wetted area and 0.1 m^3/s for the discharge.

1.4 BASEplane Specific Test Cases

1.4.1 H_BP_1: Rest Water in a closed area with strongly varying bottom

1.4.1.1 Intention

This test in two dimensions checks for the conservation of momentum. Numerical artefacts (mostly due to geometrical reasons) could generate impulse waves although there is no acting force.

1.4.1.2 Description

The computational area consists of a rectangular channel with varying bottom topography. The fluid is initially at rest with a constant water surface elevation and there is no acting force. There should be no changes of the WSE in time.

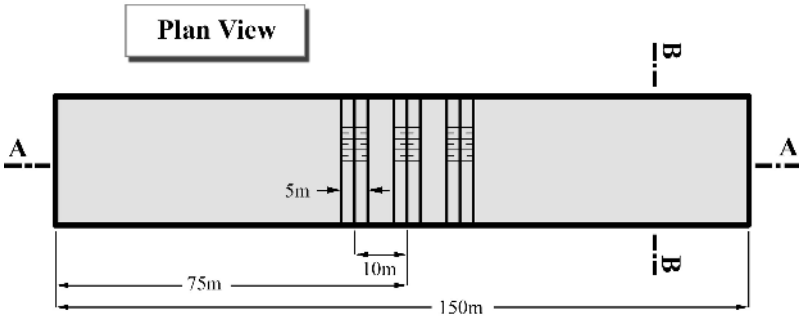

Figure 1.8 *H_BP_1: Rest Water in a closed area with strong varying bottom level, plan view*

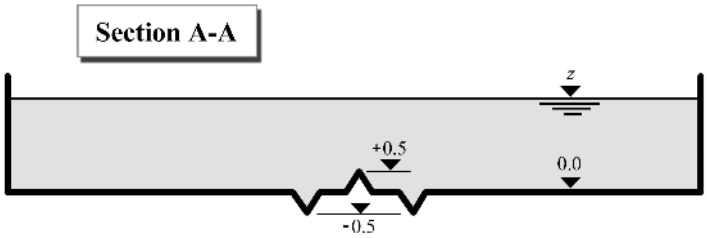

Figure 1.9 *H_BP_1: Rest Water in a closed area with strong varying bottom level, section A-A*

1.4.1.3 Geometry and Initial Conditions

Initial Condition: totally rest water, the WSE is the same and constant over the domain. The WSE can be varied e.g. from z_S (min) = 0.8 to z_S (max) 3.0 m .

1.4.1.4 Boundary Conditions

No inflow and outflow. All of the boundaries are considered as a wall.

Friction: frictionless test; Manning's factor $n = 0.0$.

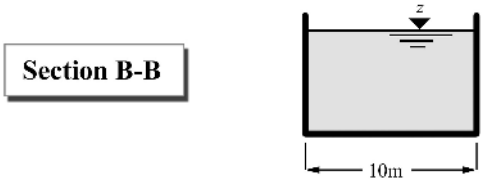

Figure 1.10 *H_BP_1: Rest Water in a closed area with strong varying bottom level, section B-B*

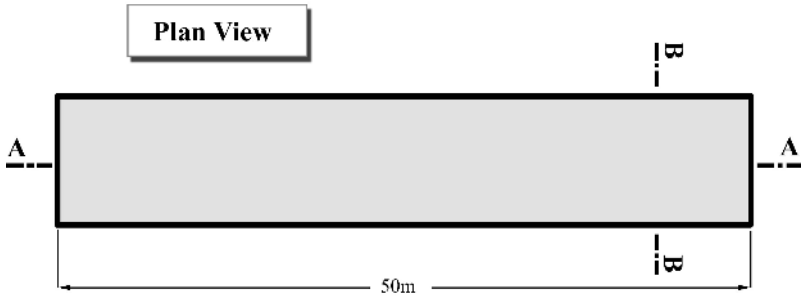

Figure 1.11 *H_BP_2: Rest Water in a closed area with partially wet elements, plan view*

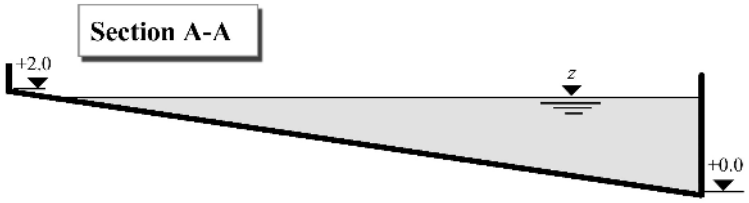

Figure 1.12 *H_BP_2: Rest Water in a closed area with partially wet elements, section A-A*

1.4.2 H_BP_2: Rest Water in a closed area with partially wet elements

1.4.2.1 Intention

This test case checks the behaviour of partially wet control volumes. The wave front respectively the border wet/dry is always the weak point in a hydraulic computation. There should be no momentum due the partially wet elements.

1.4.2.2 Description

In a sloped, rectangular channel, the WSE is chosen to be small enough to allow for partially wet elements. The water is at rest and no acting force is present.

1.4.2.3 Geometry and Initial Conditions

Initial Condition: totally rest water, the WSE is the same and constant over the whole domain. The WSE is $z_S = 1.9$ m.

1.4.2.4 Boundary Conditions

No inflow and outflow. All of the boundaries are considered as a wall.

Friction: frictionless test; Manning's factor $n = 0.0$.

The mesh (grid) can be considered as following pictures. In this form, the partially wet cells (elements) can be handled.

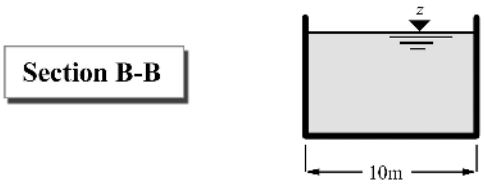

Figure 1.13 *H_BP_2: Rest Water in a closed area with partially wet elements, section B-B*

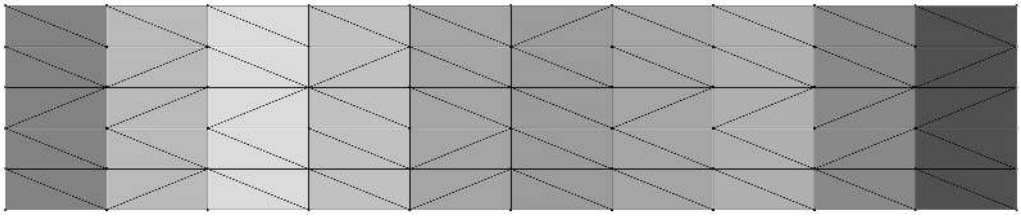

Figure 1.14 *H_BP_2: Computational grid*

1.4.3 H_BP_3: Dam break within strongly bended geometry

1.4.3.1 Intention

This test case challenges the 2-D code. The geometry permits a strongly two dimensional embossed flow. The results are compared against experimental measurements at certain control points.

1.4.3.2 Description

In a two-dimensional geometry with a jump in bed topology, a gate between reservoir and some outflow channel is removed at the beginning. The bended channel is initially dry and has a free outflow discharge as boundary condition at the downstream end.

1.4.3.3 Geometry and Initial Conditions

The geometry is described in Figure 1.16 and Figure 1.15, G1 to G6 are the measurement control points for the water elevation. Initial condition is a fluid at rest with a water surface elevation of 0.2 m above the channels ground. The channel itself is dry from water. At z =0, the gate between reservoir and gate is removed.

1.4.3.4 Boundary Conditions

No inflow. At the downstream end of the channel, a free outflow condition is employed. All other boundaries are considered as walls.

The friction factor is set to 0.0095 (measured under stationary conditions) for the whole computational domain.

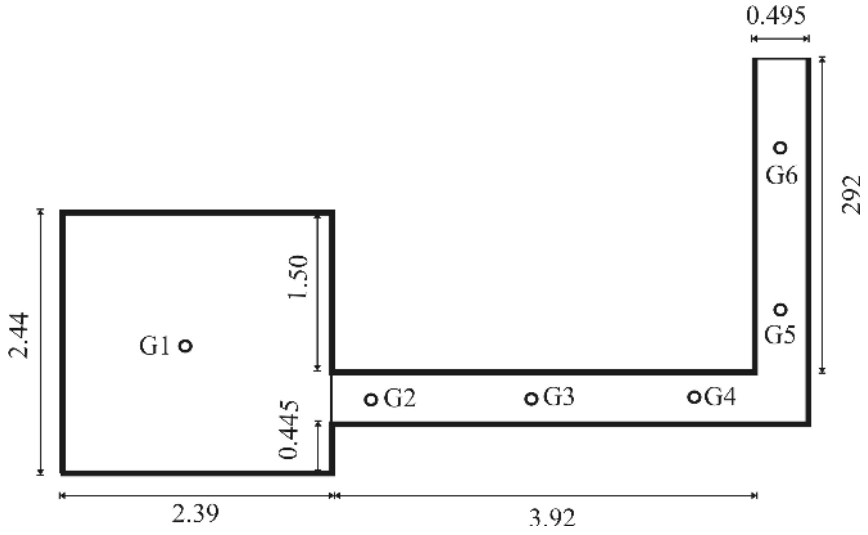

Figure 1.15 *H_BP_3: Strongly bended channel (plane view)*

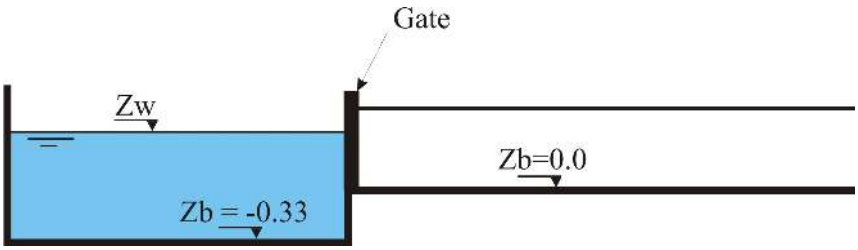

Figure 1.16 *H_BP_3: Strongly bended channel (side view)*

1.4.4 H_BP_4: Malpasset dam break

1.4.4.1 Intention

This final hydraulic test case is the well known real world data set from the Malpasset dam break in France. The complex geometry, high velocities, often and sudden wet-dry changes and the good documentation allow for a fundamental evaluation of the hydraulic code.

1.4.4.2 Description

The Malpasset dam was a doubly-curved equal angle arch type with variable radius. It breached on December 2^{nd}, 1959 all of a sudden. The entire wall collapsed nearly completely what makes this event unique. The breach created a water flood wall 40 meters high and moving at 70 km/h. After 20 minutes, the flood reached the village Frejus and still had 3 m depth. The time of the breach and the flood wave can be exactly reconstructed, as the time is known, when the power of different stations switched off.

1.4.4.3 Geometry and Initial Conditions

Figure 1.18 shows the computational grid used for the simulation. The points represent "measurement" stations. The initial water surface elevation in the storage lake is set to +100.0 m.a.s.l. and in the downstream lake to 0.0 m.a.s.l. The area downstream of the wall is initially dry. At t=0, the dam is removed.

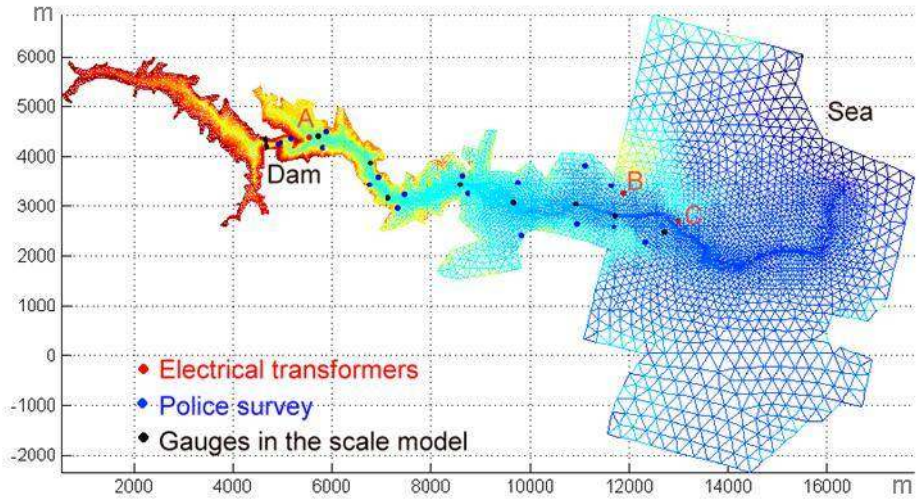

Figure 1.17 *H_BP_4: Computational area of the malpasset dam break*

1.4.4.4 Boundary Conditions

The computational grid was constructed to be large enough for the water to stay within the bounds. Friction is accounted for by a Manning factor of 0.033.

1.4.5 H_BP_5: Circular dam break wave

1.4.5.1 Intention

The circular dam break problem is a demanding two-dimensional test case with some distinct features. It is used to evaluate the capability to correctly model complex interactions of shock and rarefaction waves. The results are qualitatively compared to results obtained by Toro (2001), and other numerical studies, for this idealized dam break scenario. Also the results of the exact and approximate Riemann solvers are compared to each other.

1.4.5.2 Description

A virtual circular dam is located in the center of a computational domain. At the beginning, at time t = 0.0s, the dam is removed. The evolution of subsequent wave patterns is examined until about t = 5s after the dam break.

1.4.5.3 Geometry and Initial Conditions

The computational domain has a width and height of 40m and is modelled with a uniform rectangular grid, which consists of 160'000 quadratic elements of the size 0.1m x 0.1m. The grid is selected large enough to fully capture the outward propagating primary shock wave during the simulation time of about 5s. The small element sizes shall enable the modelling of the circular flow patterns with sufficient accuracy.

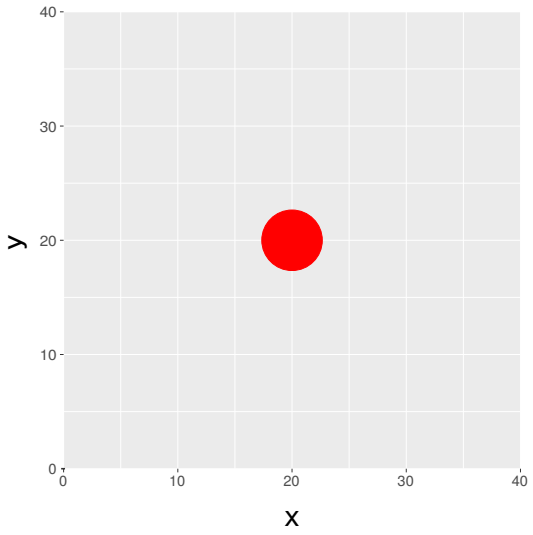

Figure 1.18 *H_BP_5: Computational area (rectangular grid) of circular dam break*

The initial height of the water column is 2.5m, whereas the surrounding initial water surface level is set to 0.5m. The water column behind the circular dam has a radius of 2.5m. The time step is chosen according to a CFL number of 0.9.

1.4.5.4 Boundary Conditions

Friction: frictionless test; Manning's factor $n = 0.0$.

1.5 Results

1.5.1 Common Test Cases

1.5.1.1 H_1: Dam break in a closed channel

The conservation of mass is validated. After $t = 1107$ s, the discharges still have a magnitude of 10^{-6} m^3/s with decreasing tendency. Both, BASEchain and BASEplane deliver similar results.

1.5.1.2 H_2: One dimensional dambreak on planar bed

1.5.1.2.1 Results obtained by BASEchain

A comparison of the 1-D test case using $h_2/h_1 = 0.000$ with the analytical solution shows an accurate behaviour of the fluid phase in time.

1.5.1.2.2 Results obtained by BASEplane

In two dimension, the dam break test case was computed using $h_2/h_1 = 0.0$ and $h_1 = 10$ m. The length of the channel was discretized using 1000 control volumes. The CFL number

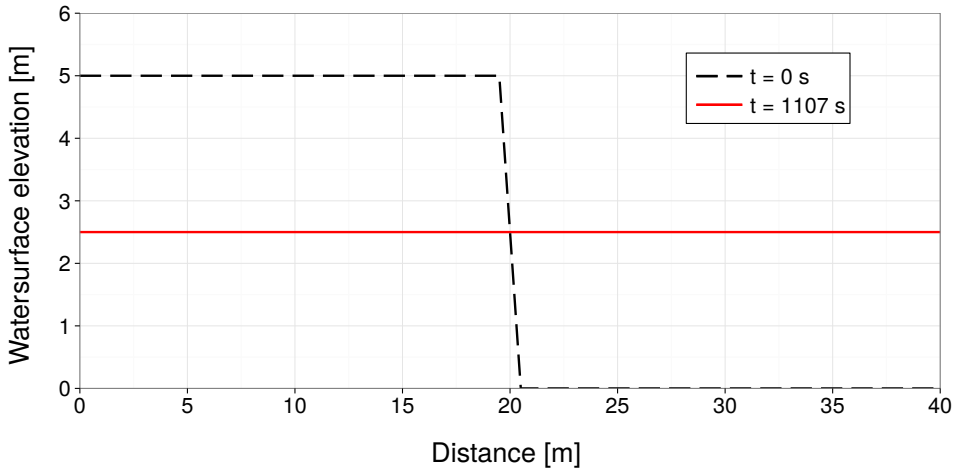

Figure 1.19 *H_1: Initial and final water surface elevation (BC & BP)*

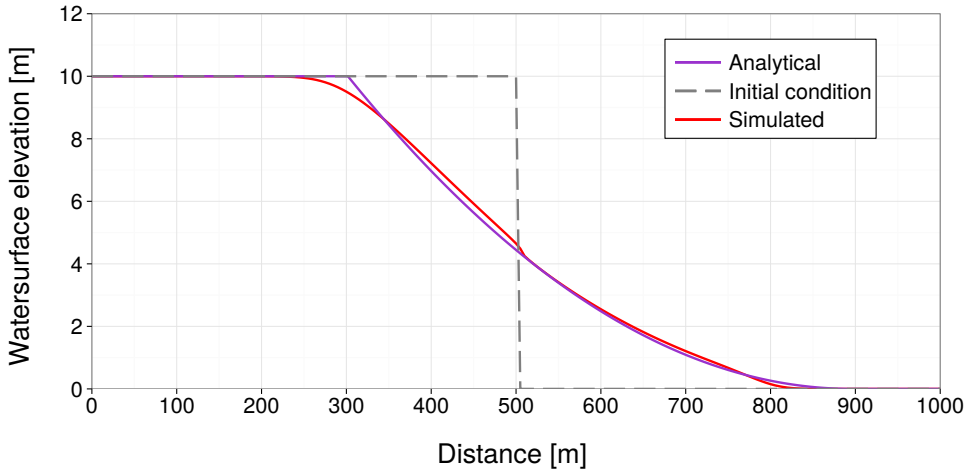

Figure 1.20 *H_2: Water surface elevation after 20 s (BC)*

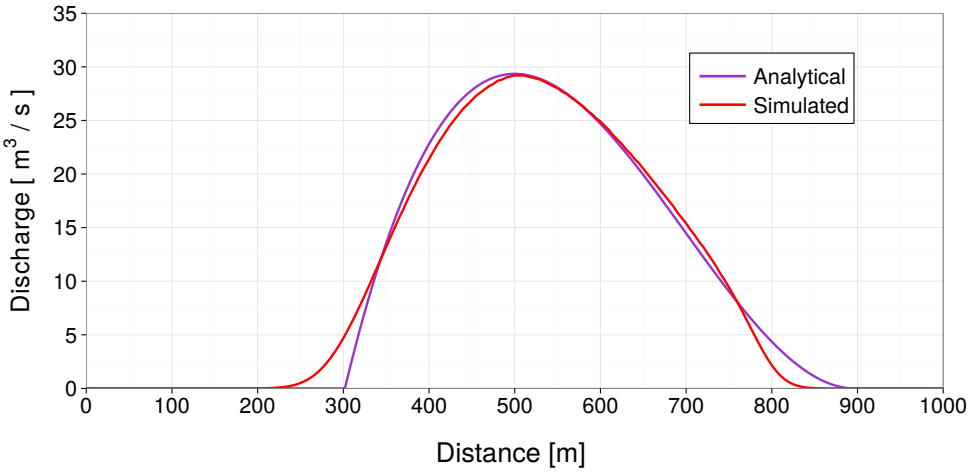

Figure 1.21 *H_2: Distribution of discharge after 20 s (BC)*

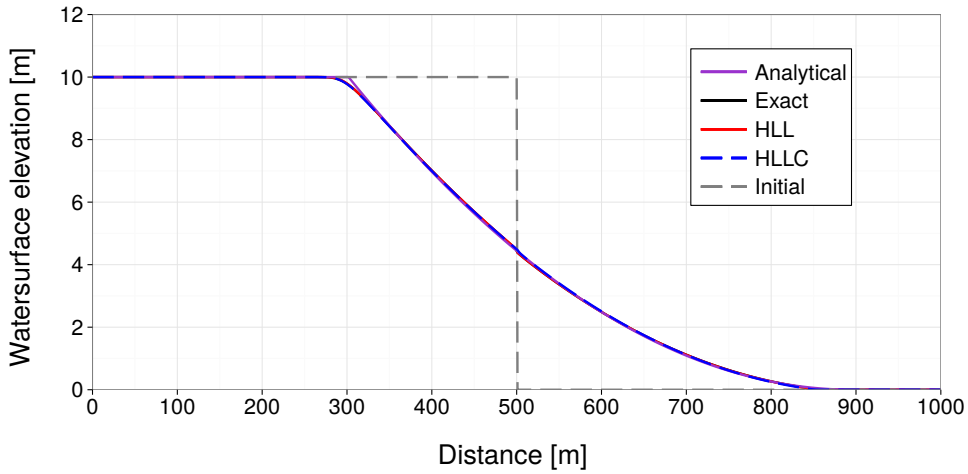

Figure 1.22 *H_2: Flow depth 20 sec after dam break (BP)*

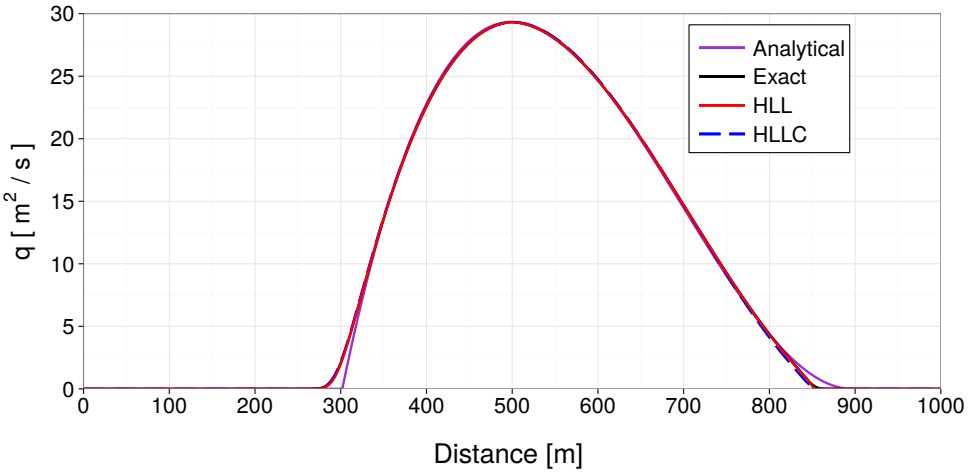

Figure 1.23 *H_2: Discharge 20 sec after dam break (BP)*

was set to 0.85. The results show a good agreement between simulation and analytical solution.

1.5.1.3 H_3: One dimensional dam break on sloped bed

1.5.1.3.1 Results obtained by BASEchain

The dam break in a sloped bed was compared against experimental results. The agreement is satisfying.

1.5.1.3.2 Results obtained by BASEplane

For two dimensions, the numerical results show a good agreement with the experimental measurements. Although in certain areas, the water depth is underestimated, the error is just at 7 % and only for a limited time. The comparison is still successful.

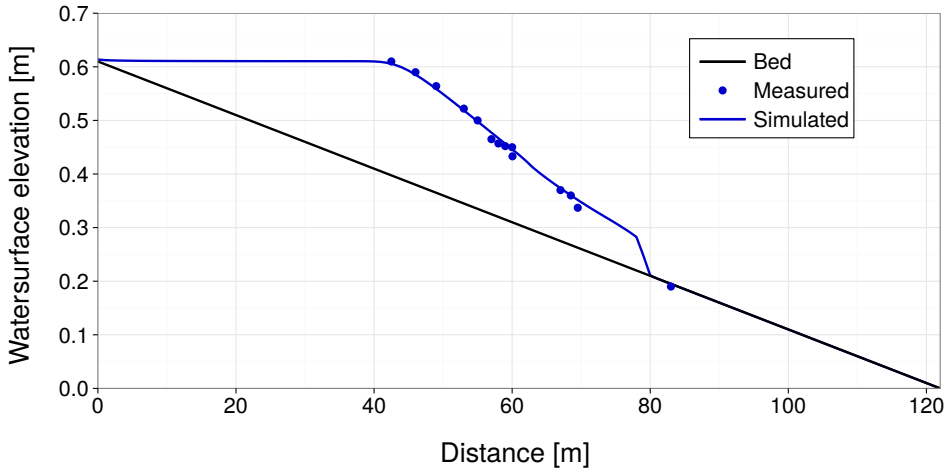

Figure 1.24 *H_3: Water surface elevation after 10 s (BC)*

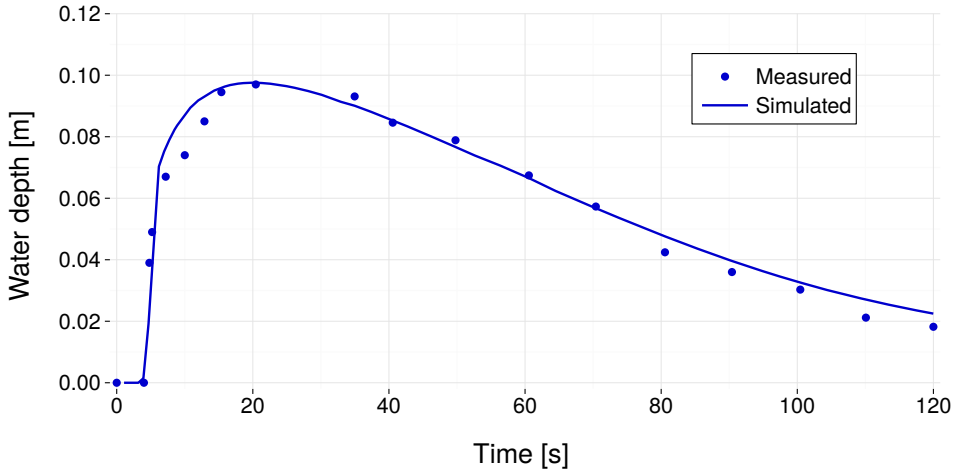

Figure 1.25 *H_3: Temporal behaviour of water depth at x = 70.1 m (BC)*

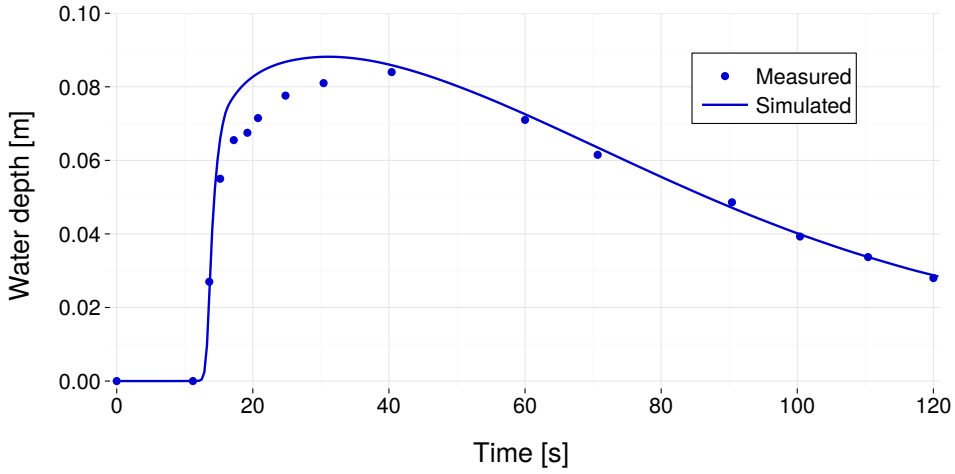

Figure 1.26 *H_3: Temporal behavior of water depth at x = 85.4 m (BC)*

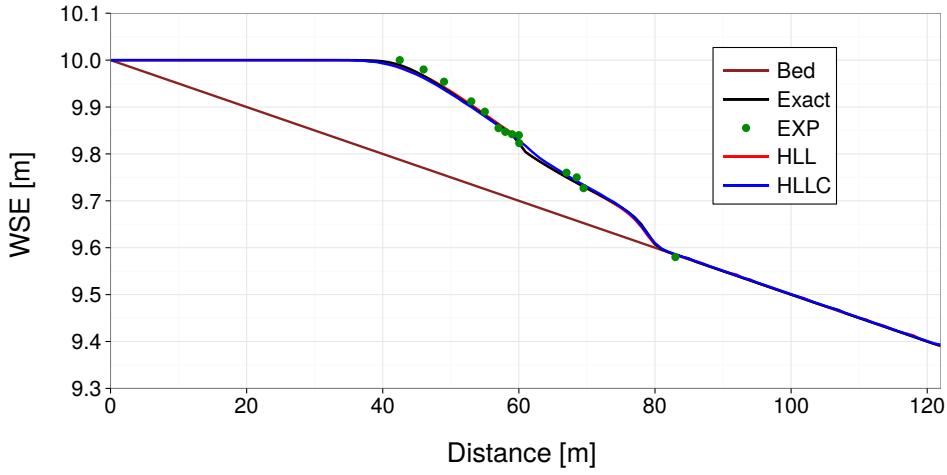

Figure 1.27 *H_3: Cross sectional water level after 10 s simulation time (BP)*

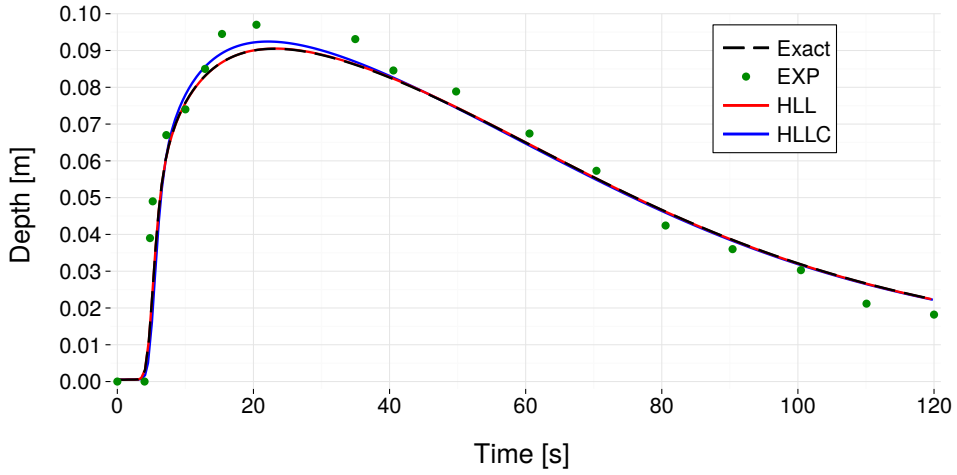

Figure 1.28 *H_3: Chronological sequence of water depth at point x = 70.1 m (BP)*

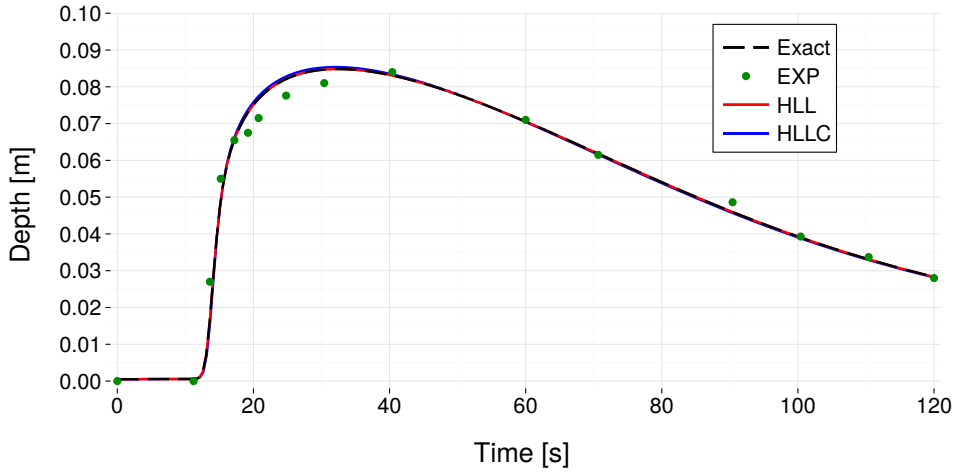

Figure 1.29 *H_3: Chronological sequence of water depth at point x = 85.4 m (BP)*

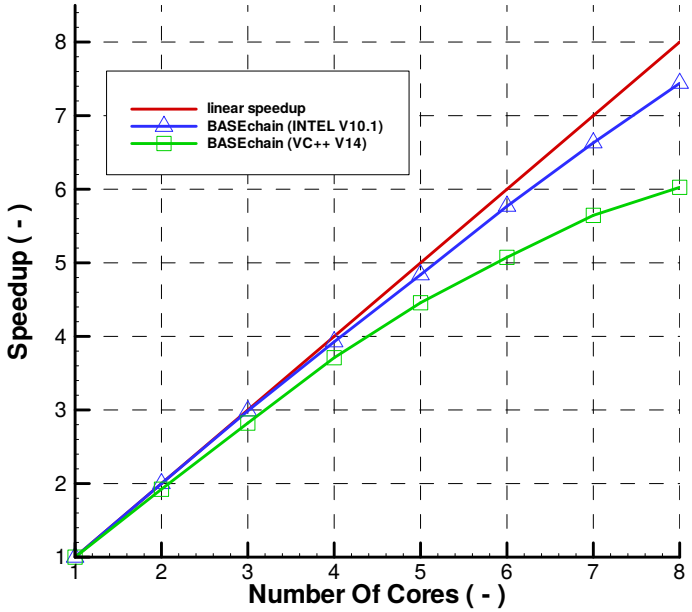

Figure 1.30 *H_4 (BASEchain) – Parallel speedup for 1-D test case*

1.5.1.4 H_4 : Parallel execution

1.5.1.4.1 General

Hydraulic simulations in a rectangular channel with steady state conditions are repeated multiple times and the execution times are measured. Thereby only the number of used threads is varied from one simulation to another. The selected model scenarios are suited well for parallel execution regarding size and load balancing in order to check the full potential of the parallel execution (in many practical model setups the observed speedups may be significantly lower).

1.5.1.4.2 System configuration

The simulations were performed an Intel multi-core shared memory system with 8 cores. The used operating system was WinXP 64.

The simulation procedure is repeated with two different versions of BASEMENT. One version (blue) is compiled with the Intel C++ compiler (V 10.1), whereas the other version (green) is compiled with the Microsoft VC++ compiler (V14).

1.5.1.4.3 Results obtained by BASEchain

The results indicate an excellent speedup and scalability. The speedup increases nearly linear with the number of used cores. The parallel speedups obtained by the Intel compiled binary are superior to those obtained by the VC++ compiled binary.

1.5.1.4.4 Results obtained by BASEplane

The results indicate a satisfactory speedup and scalability. The effect of increasing slope of the blue curve, when running this scenario with 8 cores, is probably due to caching effects. The parallel speedups obtained with the Intel compiled binary are superior to those obtained with the VC++ binary, if the number of cores exceeds 2.

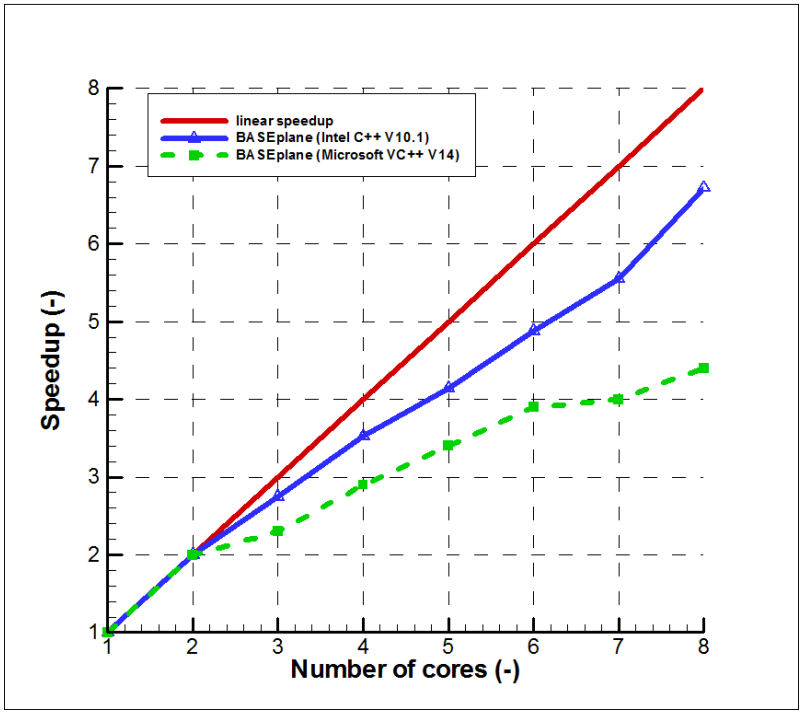

Figure 1.31 *H_4 (BASEplane) – Parallel speedup for 2-D test case*

1.5.1.5 H_5 : Controlled boundary conditions

1.5.1.5.1 Results for BASEchain

As can be seen in Figure 1.32, the controller is able to maintain the constant water level at 112.6 m precisely.

1.5.1.5.2 Results for BASEplane

Compared to the 1-D simulation, the 2-D test case is a more complicated problem as it involves discharge dependent targets and changes of discharge from 450 m^3/s down to 180 m^3/s within 5 minutes. This rapid change makes the strict maintaining of the water level difficult. In principle, this could be handled by a stronger reaction of the weir and gate, which would require also a stronger imposed upper limit of the time step to prevent numerical oscillations of the weir and gate height.

1.5.2 BASEchain Specific Test Cases

1.5.2.1 H_BC_1: Fluid at rest in a closed channel with strongly varying geometry

The test was successfully carried out. There was no movement at all – the water surface elevation remained constant over the whole area. No picture will be shown as there is nothing interesting to see.

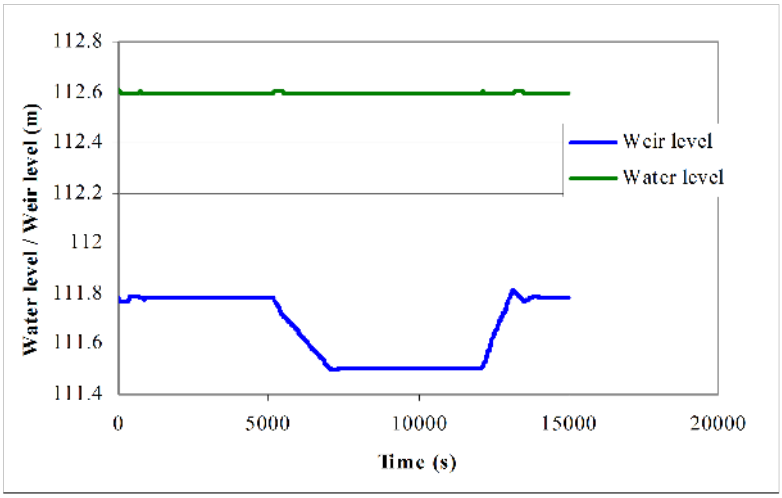

Figure 1.32 *H_5 (BASEchain) Controlled weir with changing inflow.*

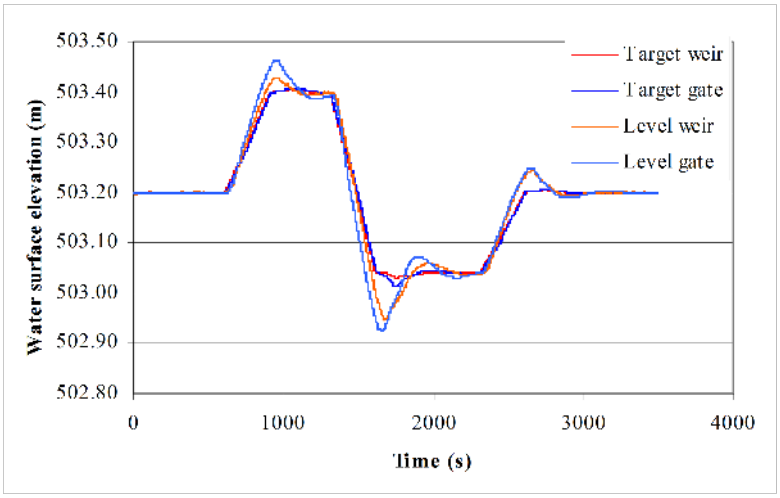

Figure 1.33 *H_5 (BASEplane) Controlled weir and gate. The target levels and the actual levels with changing inflow are given.*

1.5.2.2 H_BC_2: bed load simulation with implicit hydraulic solution

The time steps and simulation times for the explicit and implicit computations are listed in the table below. The reduction of simulation time is satisfying.

Table 1.2 *H_BC_2 : Performance of implicit calculations*

	Time step (seconds)	Simulation time (hours)	Speedup (times faster)
Explicit	2-5	13.94	
Implicit, base time step = 60	3-90	0.9	15
Implicit, base time step = 120	3-120	0.6	23
Implicit, base time step = 180	3-180	0.47	30

1.5.3 BASEplane Specific Test Cases

1.5.3.1 H_BP_1: Rest water in a closed area with strongly varying bottom

The test was successfully carried out. There was no movement at all – the water surface elevation remained constant over the whole area. No picture will be shown as there is nothing interesting to see.

1.5.3.2 H_BP_2: Rest Water in a closed area with partially wet elements

The test was successfully carried out. There was no movement at all – the water surface elevation remained constant over the whole area. No picture will be shown as there is nothing interesting to see.

1.5.3.3 H_BP_3: Dam break within strongly bended geometry

The computational area was discretized using a mesh with 1805 elements and 1039 vertices. The vertical jump in bed topography between the reservoir and the channel was modelled with a strongly inclined cell (a node can only have one elevation information). Figure 2.1 shows the water level contours and the velocity vectors. The following figures compare the time evolution of the measured water level with the simulated results at the control points G1, G3 and G5.

The results are showing an accurate behaviour expect at the control point G5, where some bigger differences can be observed. They are caused by the use of a coarse mesh around that area. Using a higher mesh density, the water level in the critical area after the strong bend is better resolved and delivers more accurate results. Figure 1.40 shows a comparison at point G5 for a coarse and a dense mesh.

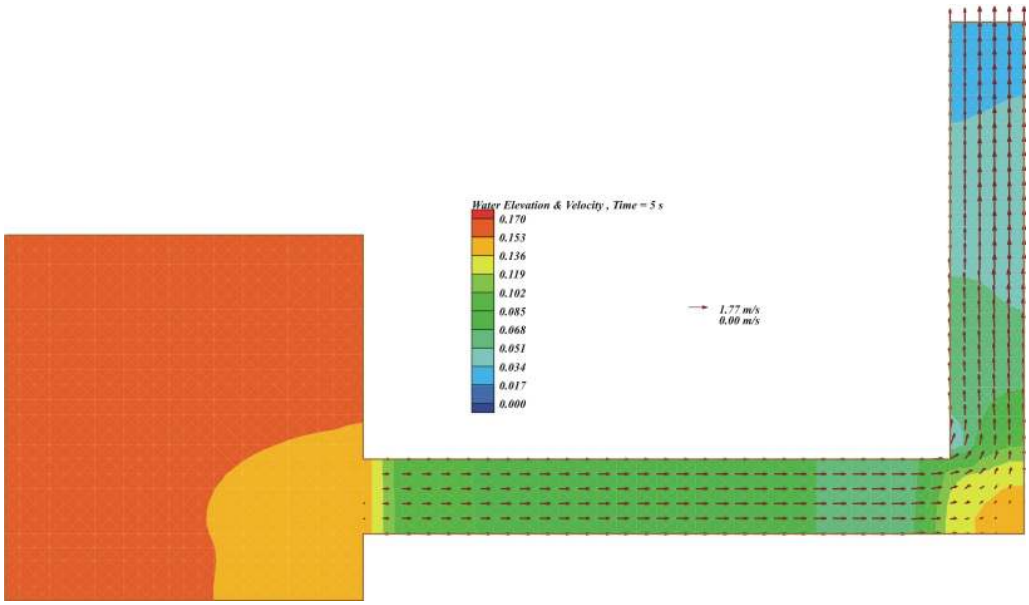

Figure 1.34 *H_BP_3: Water level and velocity vectors 5 seconds after the dam break*

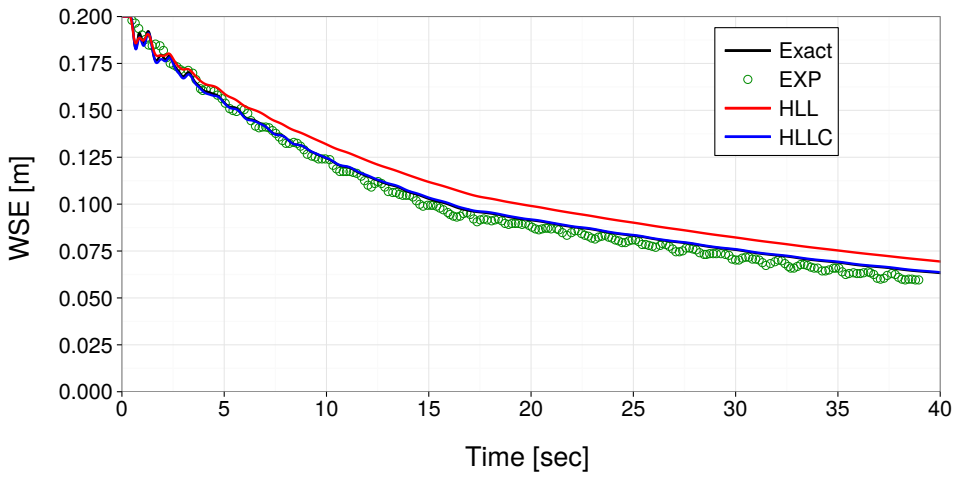

Figure 1.35 *H_BP_3: Water surface elevation at G1*

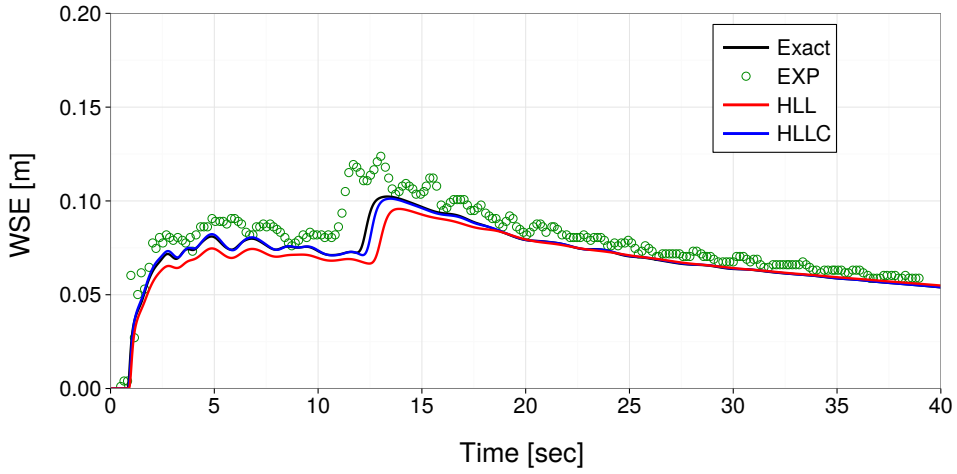

Figure 1.36 *H_BP_3: Water surface elevation at G3*

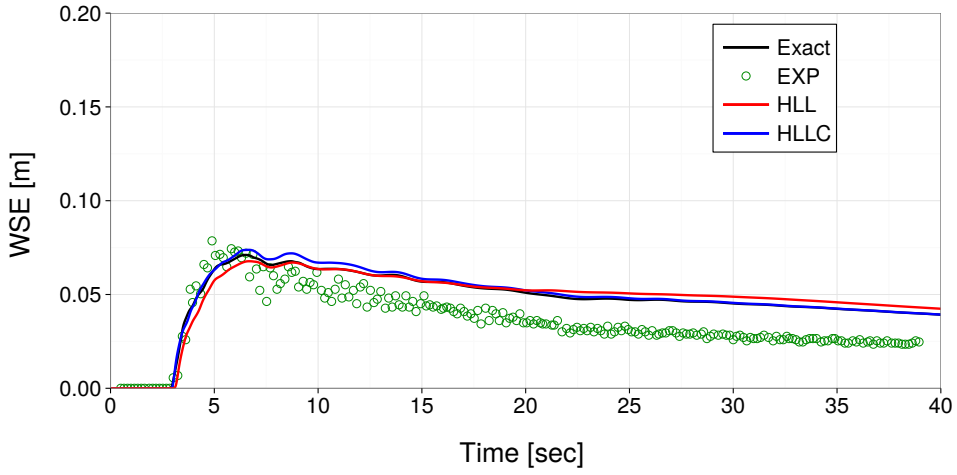

Figure 1.37 *H_BP_3: Water surface elevation at G5*

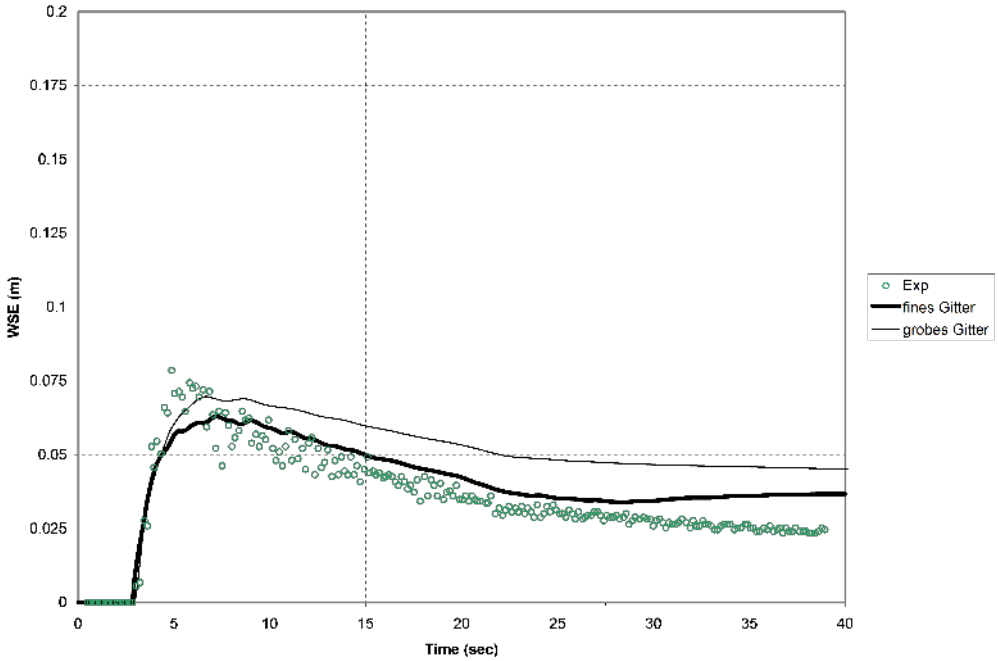

Figure 1.38 *H_BP_5: Comparison of the water level at point G5 for a coarse and a dense grid.*

1.5.3.4 H_BP_4: Malpasset dam break

The computational grid consists of 26'000 triangulated control volumes and 13'541 vertices. The time step was chosen according to a CFL number of 0.85. Figure 1.39 shows the computed water depth and velocities 300 seconds after the dam break. Figure 1.40 compares several computed with the observed data on water level elevation at different stations.

BASEplane results show a good agreement with the observed values as also other simulation results (Valiani et al. (2002) and Yoon and Kang (2004)). The differences between computed and measured data are maximally around 10%.

1.5.3.5 H_BP_5: Circular dam break

The obtained results for the circular dam break test case are plotted in two different ways. A 3-D perspective view of the depth is shown from Figure 1.41 to Figure 1.46 to illustrate the overall flow and wave patterns. Additional water surface and velocity profiles are plotted from Figure 1.47 to Figure 1.48 for distinct times.

The following flow patterns of the 2-D circular dam break are reported by Toro and other numerical studies and are also observed here.

After the collapse of dam at t = 0.0 s an outward propagating, primary shock wave is created. A sharp depth gradient develops behind this shock wave. Also, a rarefaction wave is generated which propagates inwards in the direction of the center of the dam break. The rarefaction wave finally reaches the center and generates a very distinct dip of the surface elevation at the center (t = 0.4 s) This dip travels outwards resulting in a rapid drop of the surface elevation at the center, which falls even below the initial outer water level (t = 1.4 s) and finally nearly reaches the ground (t = 3.5 s). A second shock wave develops

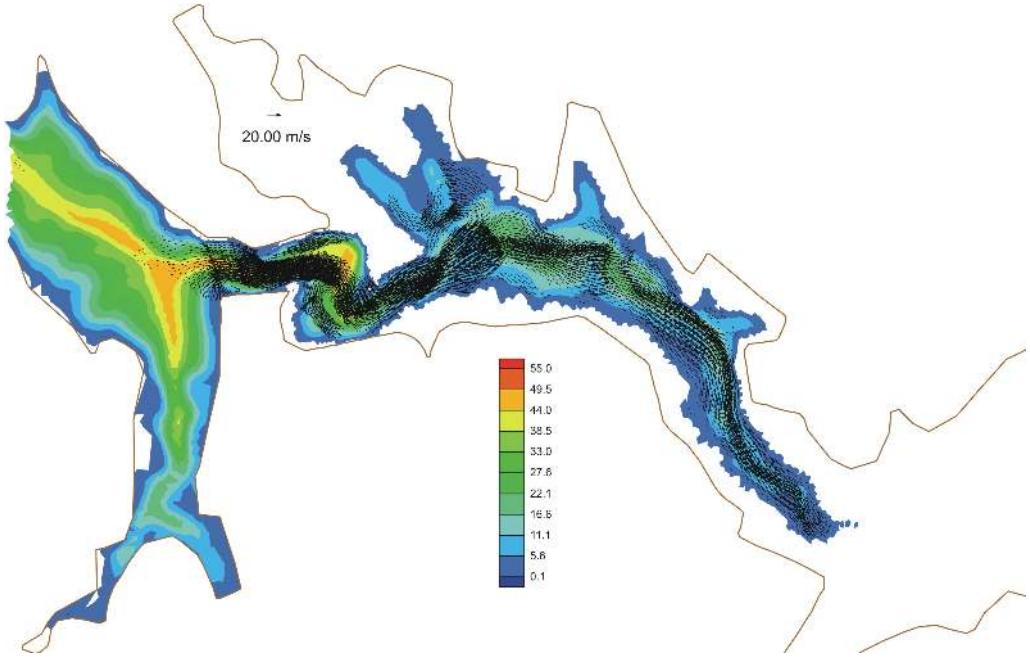

Figure 1.39 *H_BP_4: Computed water depth and velocities 300 seconds after the dam break.*

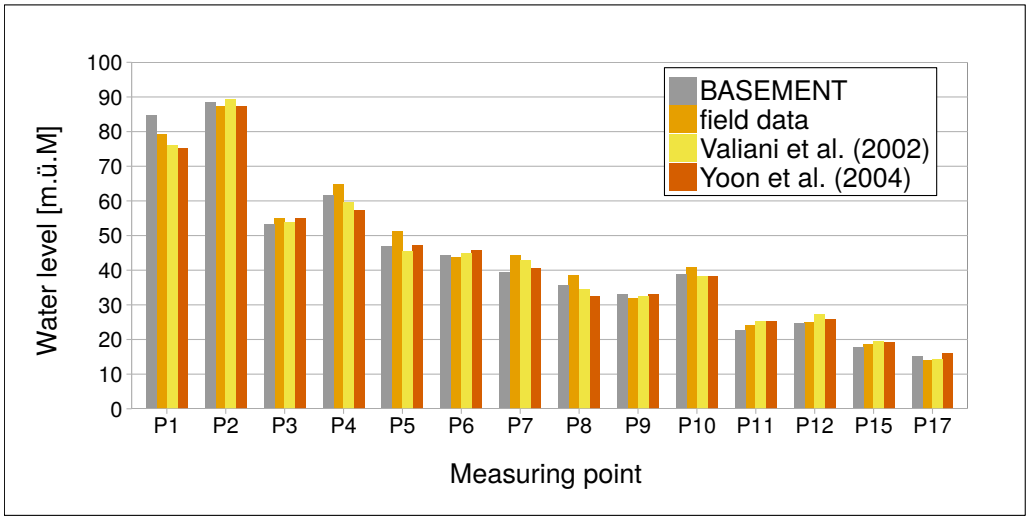

Figure 1.40 *H_BP_4: Computed and observed water surface elevation at different control points*

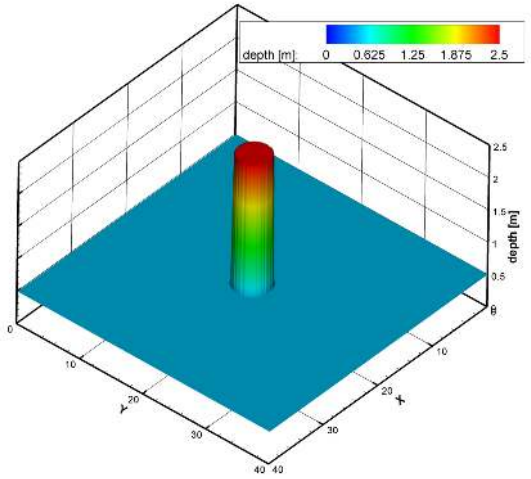

Figure 1.41 *H_BP_5: Perspective view of the circular dam break wave patterns, t=0.0s*

which propagates inwards while the primary shock wave continues to propagate outwards with decreasing strength. This secondary shock wave converges to the center and finally implodes. This generates a sharp jump in the surface water elevation at the center (t = 4.7 s).

As a result it can be stated that BASEplane is able to reproduce these distinct features of the flow and wave patterns of the 2-D circular dam break. Comparisons with the numerical results of Toro show qualitative agreement of the calculated water surface and velocities profiles. Generally, a more diffusive behaviour is observed compared to Toro's results. This may be attributed to the use of first order Godunov methods and to the use of a lower CFL number in the simulations. Despite the use of a rectangular grid, the cylindrical symmetry of the wave propagations is maintained well. Only at the first moments of the dam break, some water surface modulations can be seen at the crest of the primary shock wave which diminish with proceeding time.

The resulting water surface and velocity profiles of the approximate Riemann solvers match well the results of the exact Riemann solver. Both approximate Riemann solvers, HLL and HLLC, reproduce the flow and wave patterns.

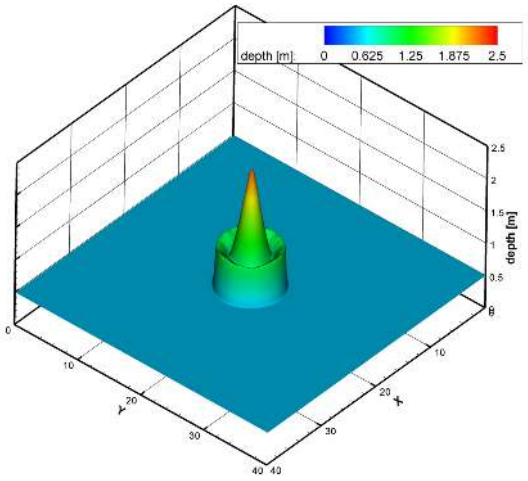

Figure 1.42 *H_BP_5: Perspective view of the circular dam break wave patterns, t=0.4s*

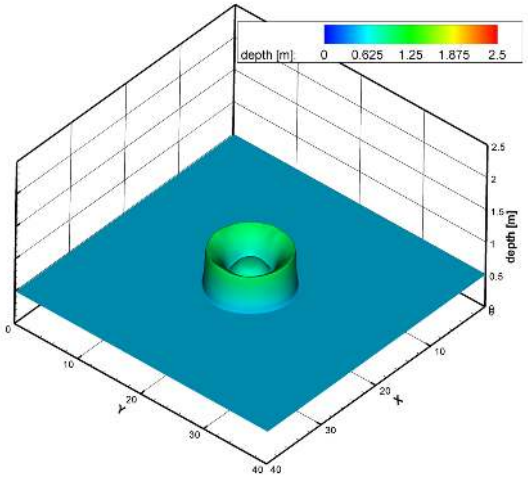

Figure 1.43 *H_BP_5: Perspective view of the circular dam break wave patterns, t=0.7s*

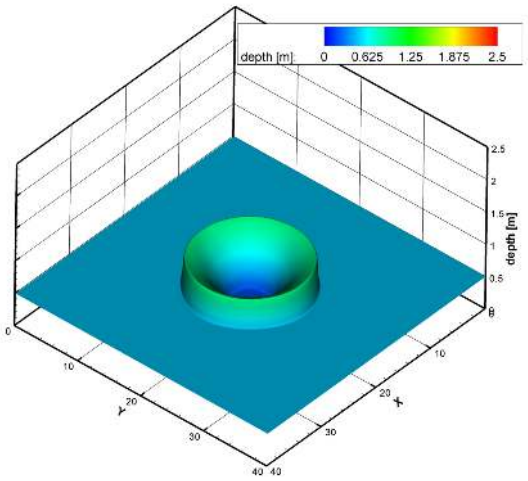

Figure 1.44 *H_BP_5: Perspective view of the circular dam break wave patterns, t=1.4s*

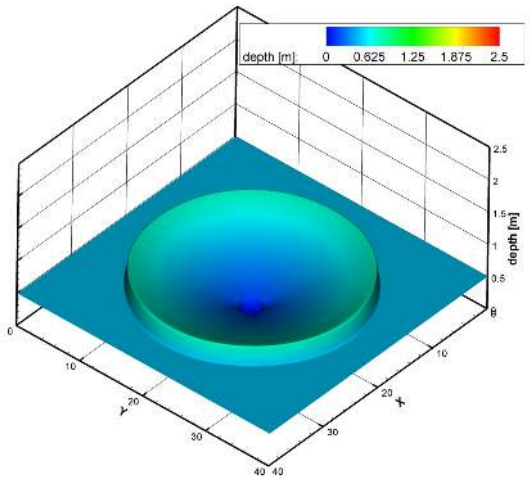

Figure 1.45 *H_BP_5: Perspective view of the circular dam break wave patterns, t=3.5s*

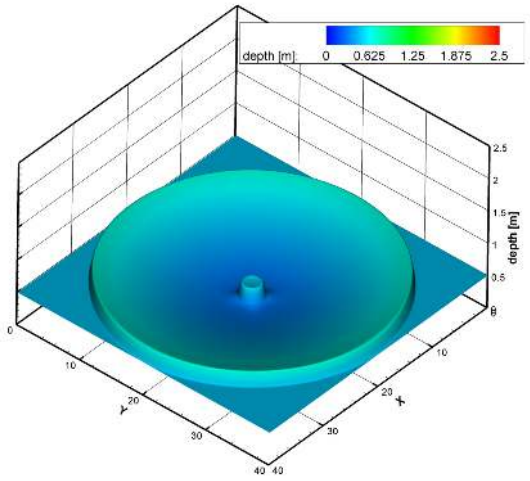

Figure 1.46 *H_BP_5: Perspective view of the circular dam break wave patterns, t=4.7s*

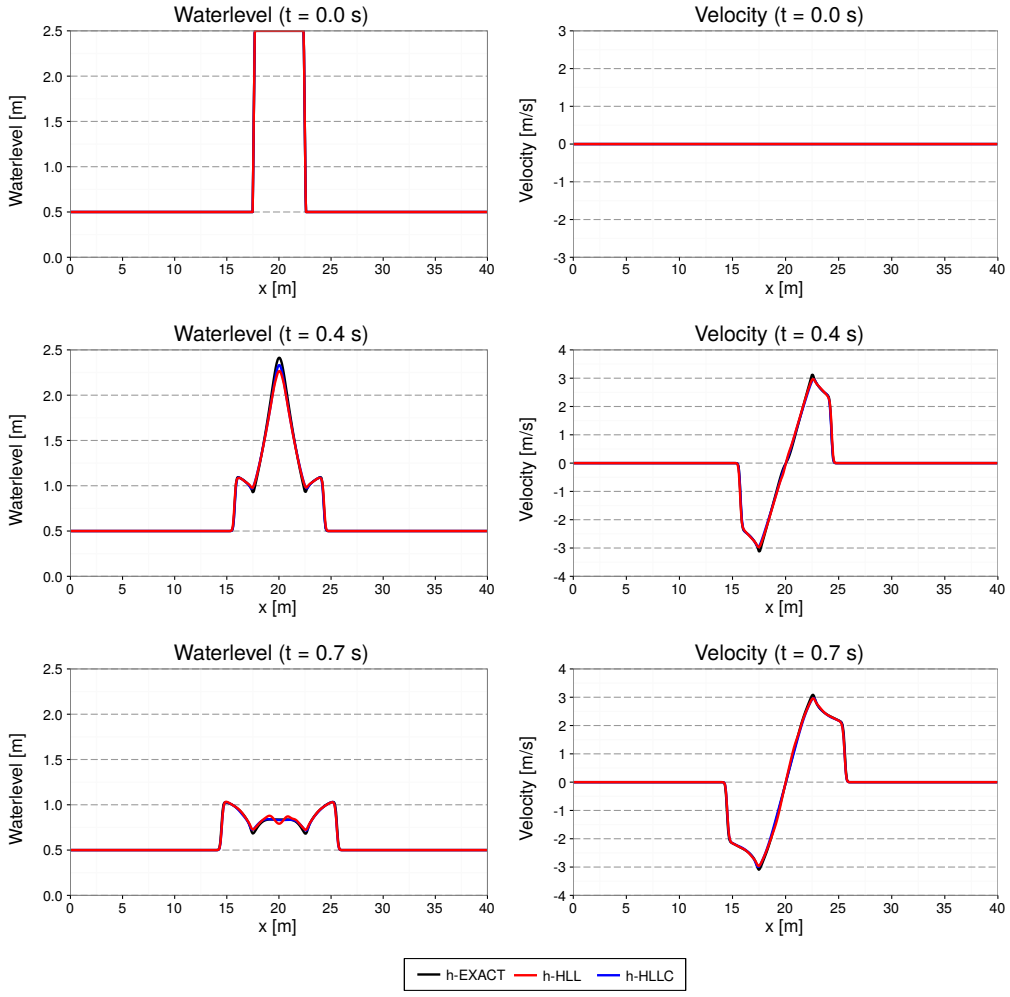

Figure 1.47 *H_BP_5: Water surface along y=20m*

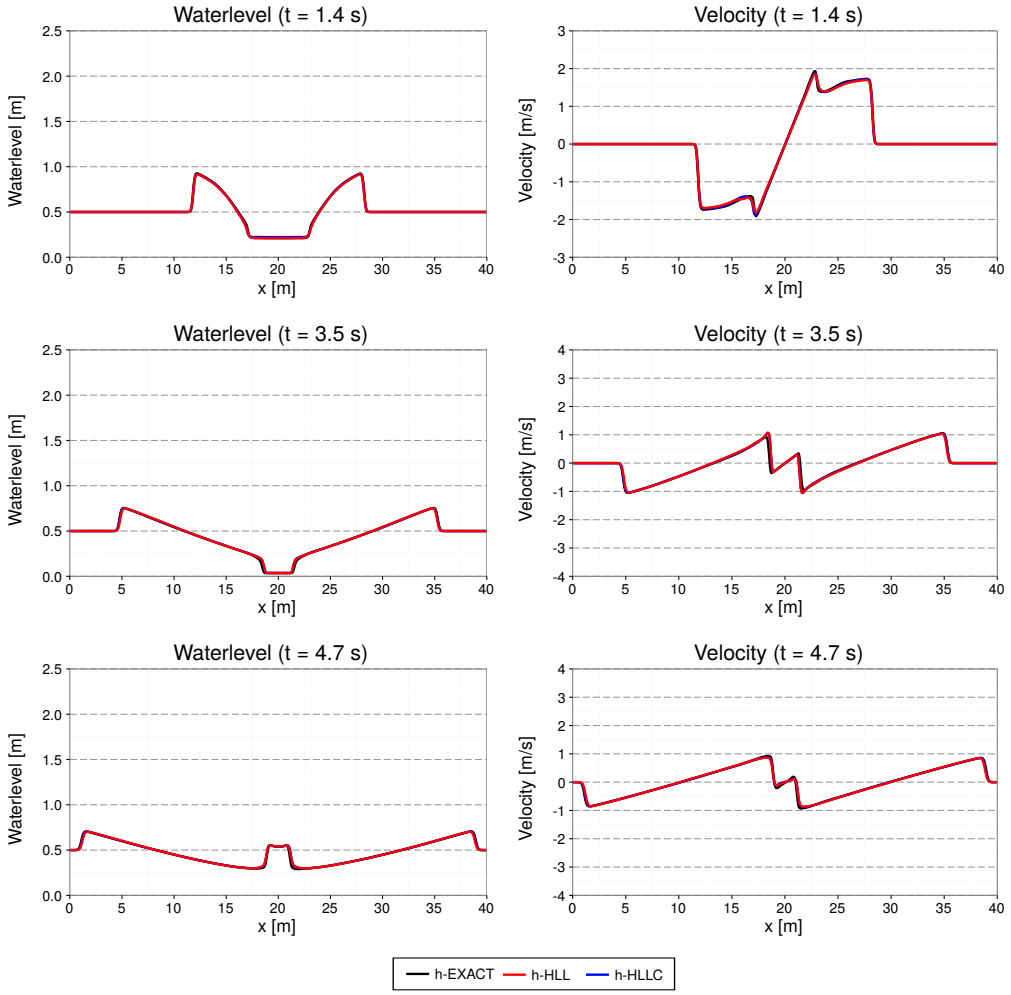

Figure 1.48 *H_BP_5: Water surface along y=20m*

2

Sediment Transport

2.1 Introduction

The test catalogue is intended for the validation of the program. The catalogue consists of different test cases, their geometric and hydraulic fundamentals and the reference data for the comparison with the computed results. The test cases are built up on each other going from easy to more and more complex problems. The sediment transport module is tested against some simple experimental test cases described in Section 2.2. Common test cases are suitable for both, 1-D and 2-D simulations. Specific test cases are intended for either 1-D or 2-D simulations.

2.2 Common Test Cases

2.2.1 ST_1: Soni et al: Aggradation due to overloading

2.2.1.1 Intention

This validation case is intended to reproduce equilibrium conditions for steady flow followed by simple aggradation due to sediment overloading at the upstream end. The test is suitable for 1-D and 2-D simulations and uses one single grain size.

2.2.1.2 Description

Soni et al. (1980) and Soni (1981) performed a series of experiments dealing with aggradations. With this particular test, they determined the coefficients a and b of the empirical power law for sediment transport. This test has been used by many researchers as validation for numerical techniques containing sediment transport phenomena (see e.g. Kassem and Chaudhry (1998), Soulis (2002) and Vasquez et al. (2005)).

The experiments were realized within a rectangular laboratory flume. First, a uniform equilibrium flow is established as starting condition. Then the overloading with sediment starts, resulting in aggradations.

2.2.1.3 Geometry and general data

Length of flume	l_f	20	[m]
Width of flume	w_f	0.2	[m]
Median grain size	d_m	0.32	[mm]
Relative density	s	2.65	[-]
Porosity	p	0.4	[-]

2.2.1.4 Equilibrium experiments

In total, a number of 24 experiments with different initial slopes S have been performed by Soni. Measured values are equilibrium water depth h_{eq} and the sediments equilibrium discharge $q_{B,eq}$. The flow velocity u_{eq} has been computed manually by Soni.

Concerning initial conditions for the equilibrium runs, "the flume was filled with sediment up to a depth of 0.15 m and then was given the desired slope". The equilibrium is reached, when a uniform flow has established respectively "when the measured bed- and water surface profiles were parallel to each other." In the average, the equilibrium needed about 4 to 6 hours to develop.

2.2.1.5 Boundary conditions

water flow: constant upstream flow discharge q_{in} and a weir on level 0 at the downstream end. Alternatively, a ghost cell may be used downstream, where the total flux into the last cell leaves the computational domain.

sediment: periodic boundary conditions are applied. The inflow $q_{B,in}$ upstream equals the outflow $q_{B,out}$ downstream.

From now on, we refer to the Soni test case #1, as the entire data for all experiments would go beyond the scope of this section. Measured data for the equilibrium are

q_{in}	4.0	$[m^3/(s \cdot m)] \times 10^{-3}$
S	3.56	$[-] \times 10^{-3}$
h_{eq}	5.0	$[m] \times 10^{-2}$
$q_{B,eq}$	12.1	$[m^3/(s \cdot m)] \times 10^{-6}$
u_{eq}	0.4	$[m/s]$

The establishment of the same equilibrium conditions is achieved by calibrating e.g. the hydraulic friction. As soon as the simulation data looks similar to the measured results, the aggradation can be started.

2.2.1.6 Aggradation experiments

After the equilibrium has been reached, the sediment feed was increased upstream by an overloading factor of $q_B/q_{B,eq}$. This factor is different for each experiment. For test case #1, it was set to 4.0. The flow discharge remains the same as in the equilibrium case. Due to the massive sediment overloading, aggradation starts quickly at the upstream end. Measured data is available for the bottom elevation at certain times.

2.2.2 ST_2 : Saiedi

2.2.2.1 Intention

Similar to the Soni test case, this validation deals with aggradation due to sediment overloading. However, compared to Soni, the sediment input is considerably greater than the carriage capacity of the flow and an aggradation shock is forming. The test verifies whether the computational model can handle shocks within the sediment phase. Again, a single grain size is used.

2.2.2.2 Description

The experiments were conducted in a laboratory flume located at the Water Research Laboratory, School of Civil Engineering, University of New South Wales, Australia. Geometric details and results are reported in Saiedi (1981a) and Saiedi (1981b). Saiedi did two separate tests, one in a steady flow and one in a rapidly unsteady flow with varying sediment supply. Only the steady case is of our interest here.

2.2.2.3 Geometry and general data

The sediment used was of fairly uniform size with the median grain size $d_{50} = 2$ mm, relative density $s = 2.6$ and porosity at bed $p = 0.37$.

The test section was about 18 m long in a 0.61 m wide glass-sided flume with a slope of 0.1 %. The flow was fed with a sediment-supply of constant rate using a vibratory feeder. The sediment input rate was chosen to be greater than the transport capacity of the flow, therefore resulting in the formation of an aggradation shock sand-wave travelling downstream. The downstream water level was maintained constant by adjusting the downstream gate.

2.2.2.4 Calibration

Before starting the sediment feed, at first, the aim is a uniform flow which fulfils a measured flow discharge q and the corresponding water depth h . This can be achieved by adjusting e.g. the hydraulic friction coefficient from Manning n. From the experiments, Saiedi proposes a calibration estimate of n=0.0136 +0.0170 q . Note that there is no sediment layer at the calibration phase.

As initial conditions, start with a fluid at rest and a uniform flow depth of h_0= 0.223 m on the sloped flume. The flow feed rate upstream is constant at $q_{in} = 0.098$ m^3/s. At the

downstream boundary, the water level is kept constant at h = 0.223 m "by adjusting the downstream gate".

2.2.2.5 Aggradation

As soon as a uniform flow with constant water depth is established, the sediment feed upstream can be started. It remains constantly on $q_B = 3.81$ kg/min. The results for the steady state computation are available at $t = 30$ min and $t = 120$ min. To avoid cluttering, the plots of the measured bed levels have been averaged.

2.2.3 BeST_3 : Guenter

2.2.3.1 Intention

The Günter test series deals with degradation in a laboratory flume. The experiments were conducted using a multiple grain size distribution. The reported results allow for a validation of the bed topography and the behaviour of heterogeneous sediment transport models.

2.2.3.2 Description

Günter performed some tests at the Laboratory of Hydraulics, Hydrology and Glaciology at the ETH Zurich using sediment input with a multiple grain size distribution. His aim was to determine a critical median shear stress of such a grain composition.

Günter was interested in the behaviour of different grain classes but also in the steady ultimate state of the bed layer, when a top layer has developed and no more degradation occurs with the given discharge. As initial state, a sediment bed with a higher slope than the slope in the steady case is used. There is no sediment feed but a constant water discharge. The bed then starts rotating around the downstream end resulting in a steady, uniform state with an armouring layer.

The validation is based on the resulting bed topography and the measured grain size distribution of the armouring layer at the end of the simulation.

2.2.3.3 Geometry and general data

Guenter actually investigated several test cases with different grain compositions and boundary conditions. This test case corresponds to his experiment No.3 with the grain composition No.1.

The experiment was conducted in a straight, rectangular flume, 40 m long, 1 m width with vertical walls. At the downstream end, the flume opens out into a slurry tank with 8 m length, 1.1 m width and 0.8 m depth (relative to the main flume), where the transported sediment material is held back. The sediment bed has an initial slope of 0.25 % with an initial grain size distribution given by

d_g [cm]	Mass fraction [%]
0.0 - 0.102	35.9
0.102 - 0.2	20.8
0.2 - 0.31	11.9
0.31 - 0.41	17.5
0.41 - 0.52	6.7
0.52 - 0.6	7.2

2.2.3.4 Simulation procedure and boundary/initial conditions

First of all, the domain gets filled slowly with fluid until the highest point is wet. The weir on the downstream end is set such that no outflow occurs. After the bed is completely under water, the inflow discharge upstream is increased successively during 10 minutes up to the constant discharge of 56.0 l/s. At the same time, the weir downstream is lowered down to a constant level until the water surface elevation remains constant in the outflow area. There is no sediment inflow during the whole test.

Using this configuration, the bed layer should rotate around the downstream end of the soil. The experiment needed about 4 to 6 weeks until a stationary state was reached. The data to be compared with the experiment are final bed level and final grain size distribution.

2.3 BASEchain Specific Test Cases

2.3.1 ST_BC_1: Advection of suspended load

2.3.1.1 Intention

This test is intended to verify the quality of the advection schemes. The aim is to minimize the numerical diffusion even over long distances.

2.3.1.2 Description

In a rectangular channel with steady flow conditions the advection of the suspended material is observed, once for a vertical front of concentration (case A) and once for a concentration with a Gaussian distribution (case B). The Quickest, Holly-Preissmann and MDPM-Scheme are tested. The diffusion is set to 0 and there is no sediment exchange with the soil.

2.3.1.3 Geometry and initial conditions

- The computational area is a rectangular channel with 10 km length, 30 m width and a slope of 0.5 ‰ .The cell width Δx is 40 m.
- The initial condition for the hydraulics is a steady discharge of 10 m^3/s
- The initial conditions for the suspended load are the following:

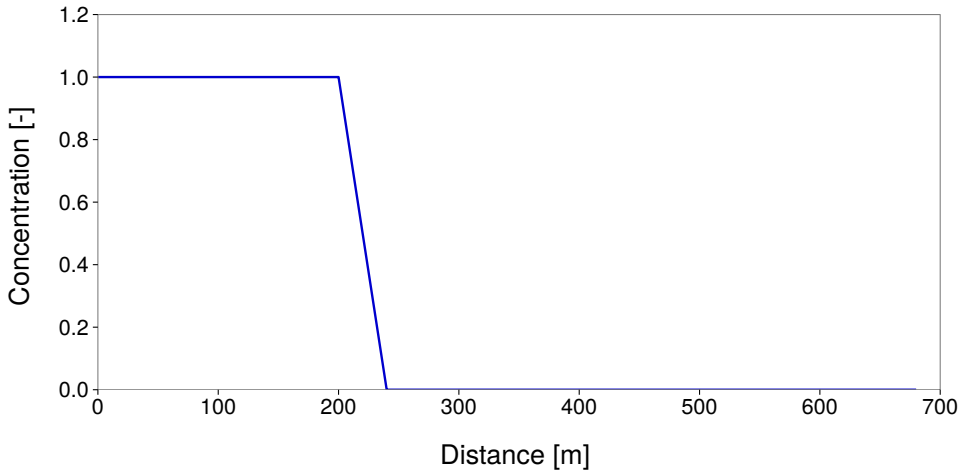

Figure 2.1 *ST_BC_1: Initial condition for case A*

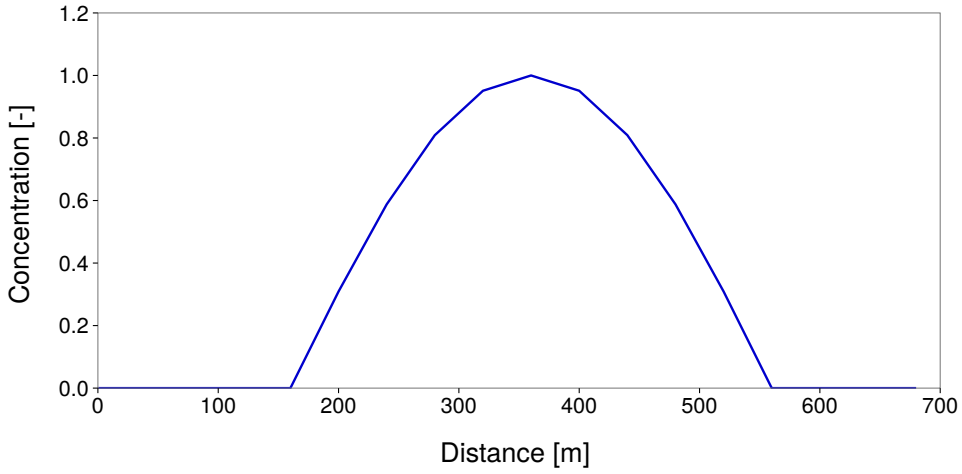

Figure 2.2 *ST_BC_1: Initial condition for case B*

Case A: The concentration is 1 for the first 200 meters of the flume and 0 for the rest.

Case B: The concentration has a Gauss-distribution on the upstream part of the flume.

2.3.1.4 Boundary conditions

- The friction expressed as k_{Str} is 80.
- The hydraulic upper Boundary is a hydrograph with steady discharge of 10 m^3/s.
- The hydraulic outflow boundary is h-q-relation directly computed with the slope.
- The upper boundary condition for suspended load is a constant inflow concentration of 1 for case A and 0 for case B.
- The lower boundary condition is an outflow concentration corresponding to the concentration in the last cell.

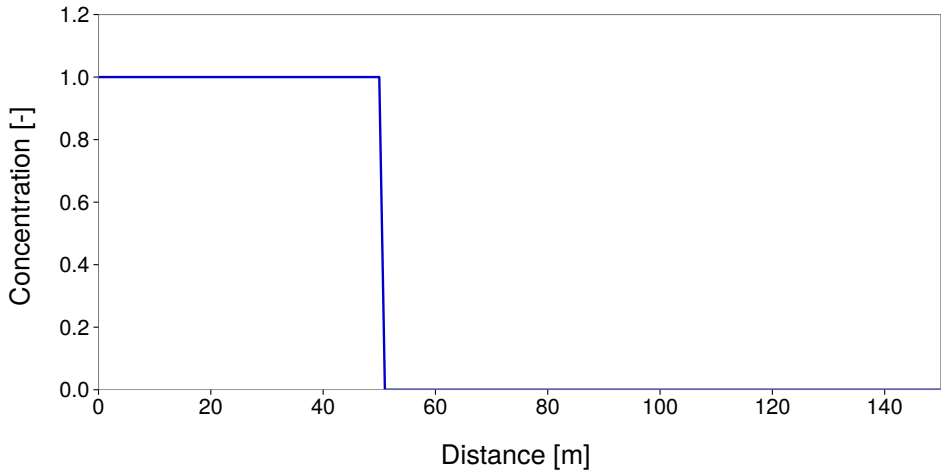

Figure 2.3 *ST_BC_2: Initial condition for case A*

2.3.2 ST_BC_2: Advection-Diffusion

2.3.2.1 Intention

This test is intended to verify the combination of advection and diffusion for suspended load for a given diffusion factor Γ.

2.3.2.2 Description

In a rectangular channel with steady flow conditions the behaviour of the suspended material is observed, once for a vertical front of concentration (case A) and once for a concentration with a Gaussian distribution (case B). The Quickest, Holly-Preissmann and MDPM-Scheme are tested. There is no sediment exchange with the soil.

2.3.2.3 Geometry and initial conditions

- The computational area is a rectangular channel with 1000 length, 20 m width and a slope of 1 ‰. The friction expressed as k_{Str} is 30. The cell width Δx is 1 m.
- The initial condition for the hydraulics is a steady discharge of 50 m^3/s.
- The initial conditions for the suspended load are:

Case A: The concentration is 1 for the first 50 meters of the flume and 0 for the rest.

Case B: The concentration has a Gauss-distribution on the upstream part of the flume.

2.3.2.4 Boundary conditions

- The friction is expressed as k_{Str} is 30.
- The hydraulic upper boundary is hydrograph with steady discharge of 50 m^3/s.
- The hydraulic outflow boundary is h-q-relation directly computed with the slope.

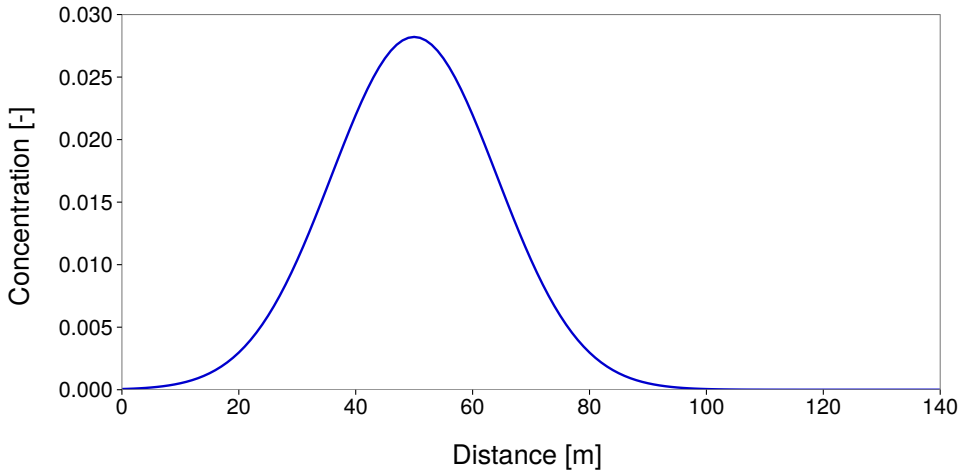

Figure 2.4 *ST_BC_2: Initial condition for case B*

- The upper boundary condition for suspended load is a constant inflow concentration of 1 for case A and 0 for case B.
- The lower boundary condition is an outflow concentration corresponding to the concentration in the last cell.

2.4 BASEplane Specific Test Cases

2.4.1 ST_BP_1: Advection of suspended load

2.4.1.1 Intention

This test is intended to verify the quality of the advection scheme. The aim is to minimize the numerical diffusion even over long simulation time or distance.

2.4.1.2 Description

In a rectangular channel with steady flow conditions the advection of the suspended material is observed, once for a vertical front of concentration (case A) and once for a concentration with a Gaussian distribution (case B). The MDPM-Scheme is tested. The diffusion is set to 0 and there is no sediment exchange with the soil.

2.4.1.3 Geometry and initial conditions

- The computational area is a rectangular channel with 1 km length, 10 m width and a slope of 7 ‰.
- The initial condition for the hydraulics is a steady discharge of 50 m^3/s.
- The initial conditions for the suspended load are the following:

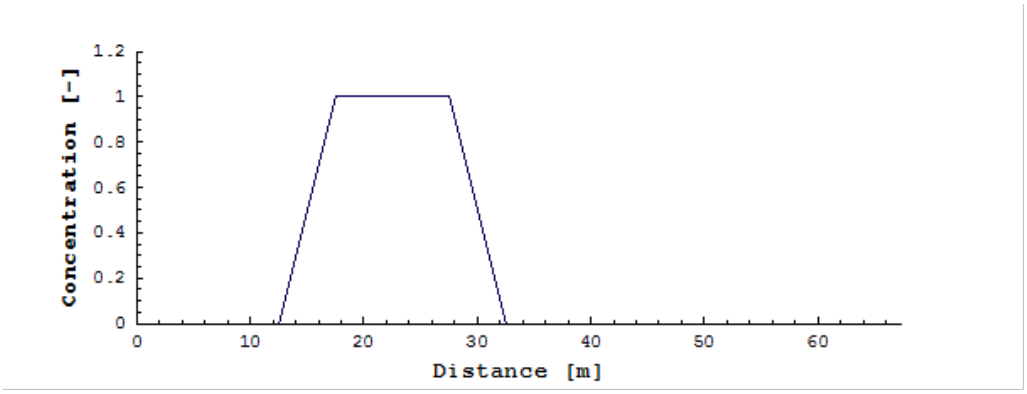

Figure 2.5 *ST_BP_1: Initial condition for case A*

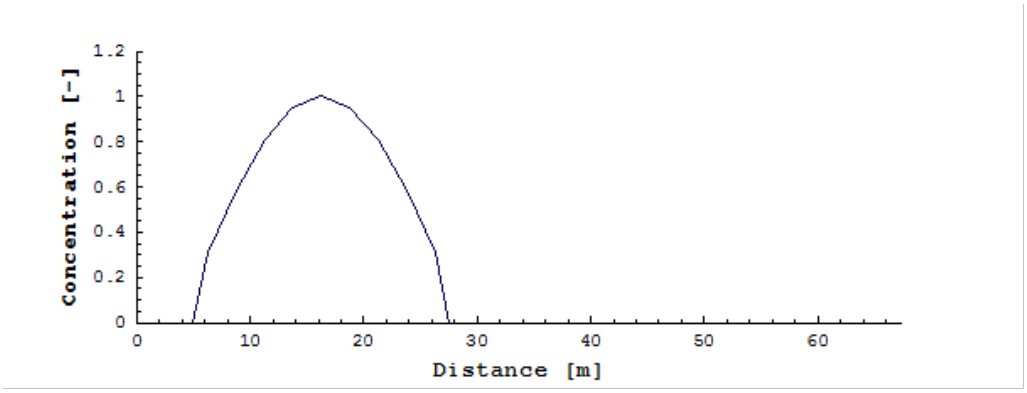

Figure 2.6 *ST_BP_1: Initial condition for case B*

Case A: The concentration is 1 for the first 30 meters at the upper end of the channel. During the simulation a constant sediment source is added to maintain between 15 and 20 meters from the upstream end to maintain a constant concentration.

Case B: The concentration has a Gauss-distribution on the upstream part of the flume.

2.4.1.4 Boundary conditions

- The friction is expressed as Manning factor n is 0.03.
- The upper boundary is a hydrograph with steady discharge of 50 m^3/s with concentration 0.
- The hydraulic outflow boundary is zero_gradient.
- The lower boundary condition for suspended load is an outflow concentration corresponding to the concentration in the last cell.

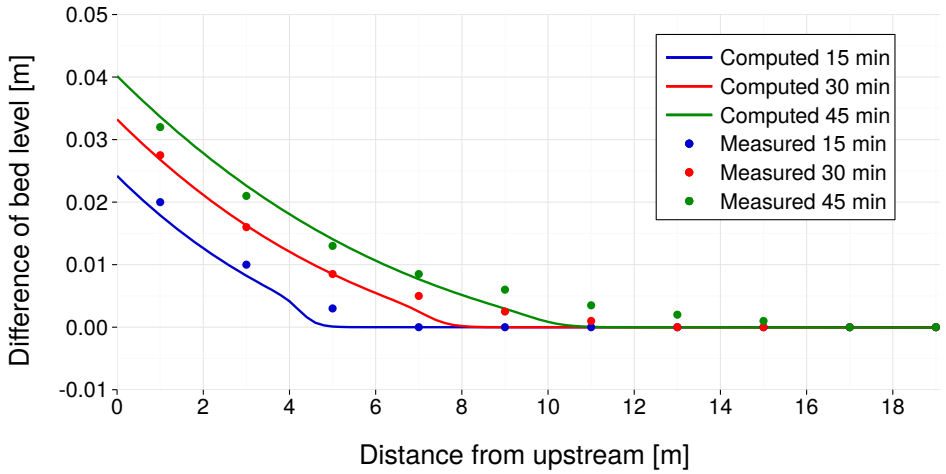

Figure 2.7 *Soni Test with MPM-factor = 6.44 (BC)*

2.5 Results

2.5.1 Common Test Cases

2.5.1.1 ST_1: Soni

2.5.1.1.1 Results obtained by BASEchain

The Soni test case has been simulated with the MPM approach like the one used for the next test case of Saiedi (see Section 2.2.2). As the equilibrium bed load of 2.42· 10^{-7} m^3/s is known, the MPM-factor has been calibrated to obtain a good agreement for the equilibrium state. This leads to a value of 6.44 for the prefactor in the MPM-formula.

The results show a quite good agreement between experiment and simulation.

2.5.1.1.2 Results obtained by BASEplane

The Soni test case was modelled as single grain computation on a mobile bed with the transport formula of Meyer-Peter & Müller (MPM). The grain diameter is chosen as the mean diameter of the grain mixture used by Soni. The simulations were performed on an unstructured mesh with 1202 triangular elements.

In Soni's experiments at first an equilibrium transport was established within the laboratory flume. The corresponding transport rate observed by Soni is known to be 2.42*10^{-7} m^3/s. Then the sediment inflow was increased to 4 times the equilibrium transport.

To be able to reproduce the experiments, the transport formula must be calibrated to achieve the same equilibrium transport rate. The calibration resulted in a reduction of the pre-factor of the MPM formula from 8 to about 3.3. The critical dimensionless shear stress for incipient motion in the MPM formula is not calibrated here and therefore, per default, determined from the Shields diagram.

The numerical results for the bed aggradations and the water levels are compared with the measurements by Soni. The situations after 15min, 30min and 40min are plotted in the following figures. Generally the numerical results show an acceptable agreement

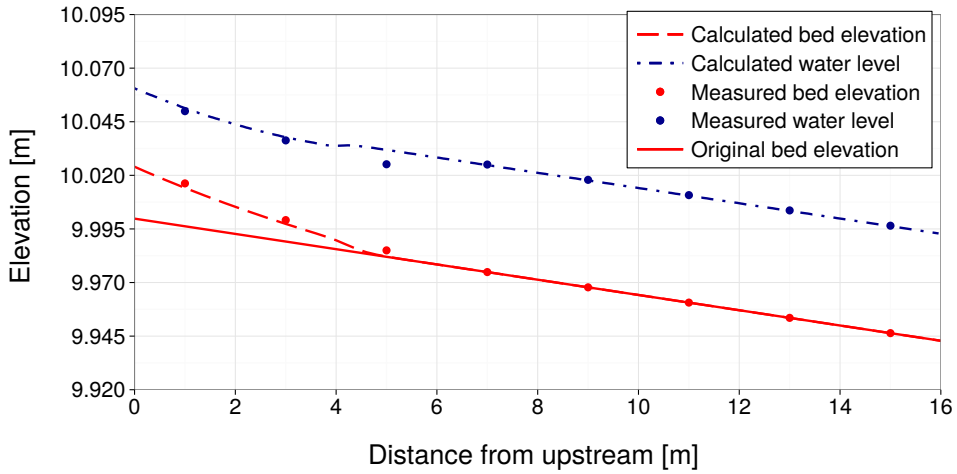

Figure 2.8 *ST_1: Soni Test – Bed aggradation and water level after 15 min (BP)*

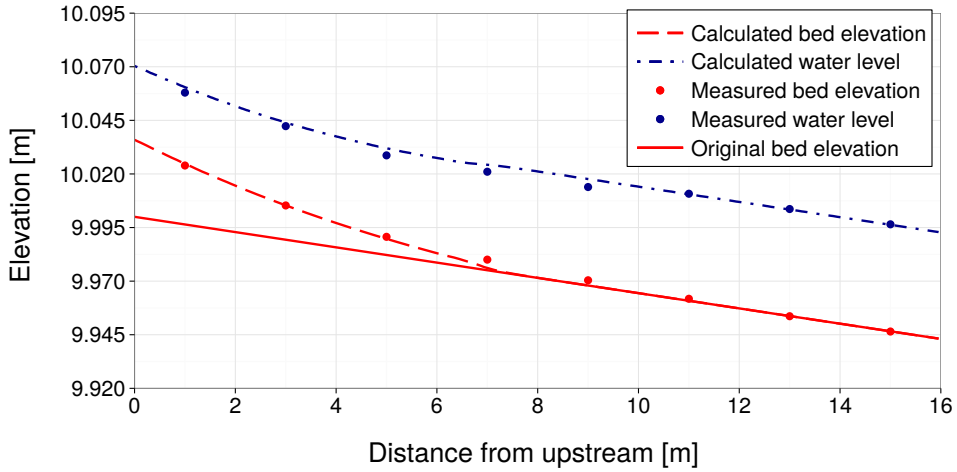

Figure 2.9 *ST_1: Soni Test – Bed aggradation and water level after 30 min (BP)*

with the measured values. Compared to the measurements, the toe of the aggradation front shows a less diffusive smearing behaviour. This may be attributed to the finer grain fractions within Soni's grain mixtures, whose behaviour is not adequately modelled in single grain computation. Also the rather fine diameter of 0.32 mm can be seen as problematic concerning the applicability of the MPM formula, which is best suited for coarse sands and gravel.

2.5.1.2 ST_2: Saiedi

2.5.1.2.1 Results obtained by BASEchain

The Saiedi test was simulated using the Meyer-Peter Müller approach for the sediment flux, which can also be formulated as:

$q_B = factor(\theta - \theta_{cr})^{3/2}\sqrt{(s-1)g}d_m^{3/2}$

The factor is usually set around 8.0 and should be between 5 and 15 (Wiberg and Smith,

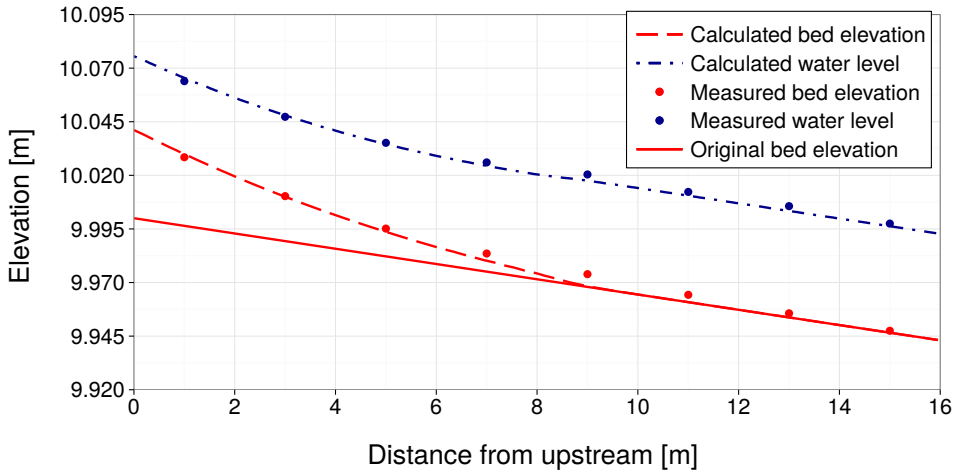

Figure 2.10 *ST_1: Soni Test – Bed aggradation and water level after 40 min (BP)*

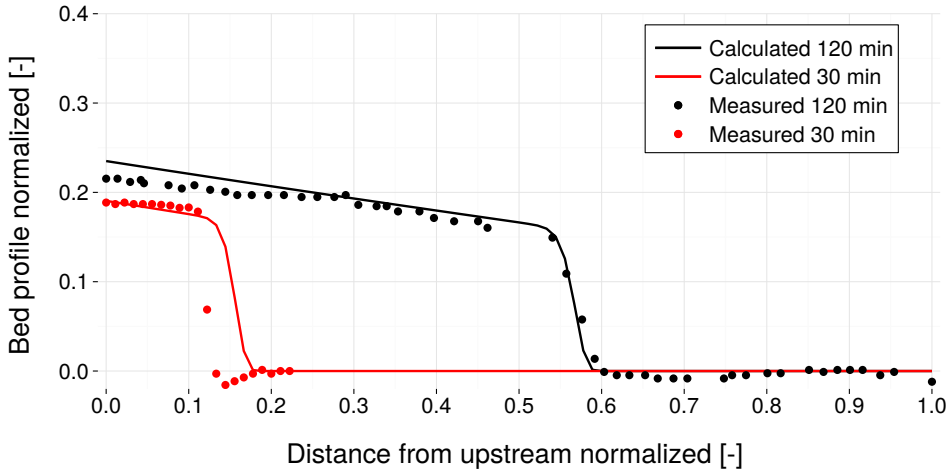

Figure 2.11 *Saiedi Test, with MPM-factor = 13 (BC)*

1989). In this case it was calibrated to 13.

The results present a good fit. This example shows that, to reproduce this type of transport, the approach of MPM approach needs calibration.

2.5.1.2.2 Results obtained by BASEplane

The Saiedi test case was simulated using a single grain approach on an unstructured mesh made of 768 triangles. The Meyer-Peter & Müller formula was used to determine the bedload transport. The simulation was performed on a fixed bed, where no erosion can take place.

To obtain a reasonable fit between the measured values and the simulation results the pre-factor of the transport formula again had to be reduced from 8 to about 5. Furthermore, the simulations show that the sediment is transported too rapidly out of the flume compared to the experiments. To compensate for this effect the critical Shields factor for incipient motion is increased to 0.055, instead of using the value from the Shields diagram.

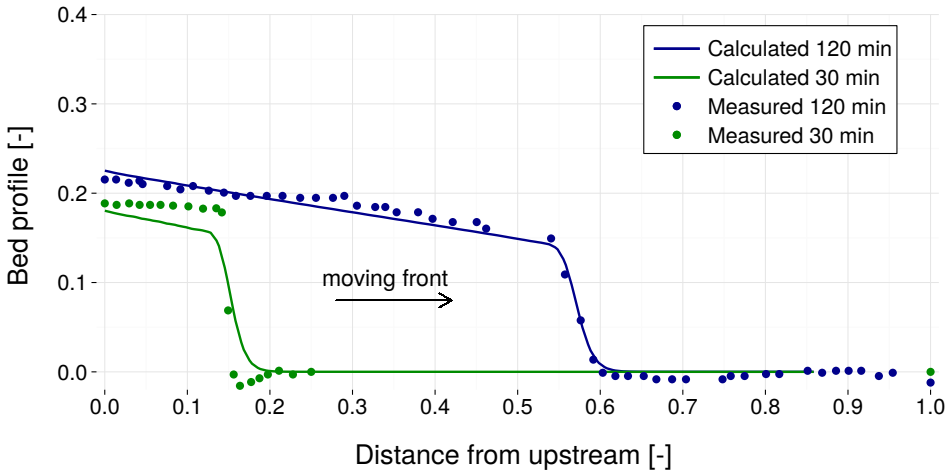

Figure 2.12 *ST_2 : Saiedi Test, propagation of sediment front (BP)*

With these adjustments, the shape and the propagation speed of the sediment front are captured well and Saiedi's results can be reproduced with good accuracy. The front of the sediment bore does not smear over the time but remains steep during the propagation.

2.5.1.3 ST_3: Guenter

2.5.1.3.1 Results obtained by BASEchain

For mixed materials, the Guenter test case has been performed. The initial slope was chosen to be 0.25 % - this corresponds to the full experiment of Guenter.

The eroded material is eliminated from the end basin by a sediment sink. The active layer height is 5 mm and the critical dimensionless shear stress (for beginning of sediment transport) is set to the default value of 0.047. After 200 hours, there are no more important changes recognizable. After the results of Guenter the slope at the final equilibrium state should be the same as the initial one.

The final slope in the numerical model is in good agreement with the final slope observed in the physical experiment. Moreover the grain sorting effect can be modelled quite well. The final grain size distribution is slightly coarser than the observed grain size distribution in the physical model (Figure 2.14).

There are many parameters which influence this result, especially the choice of the critical shear stress and the active layer thickness. Again, this example shows, one has to use different approaches for sediment transport with different values for the free parameters. Quite often, a sensitivity analysis may give a better insight in the behaviour of certain formulas and their parameters.

2.5.1.3.2 Results obtained by BASEplane

The Guenter test has been numerically modelled with 6 different grain classes. The sediment transport capacity has been determined with Hunziker's formula for graded transport. The critical dimensionless shear stress for beginning of sediment transport is set to the default value of 0.047 in Hunziker's formula. This bedload formula was not further adjusted for

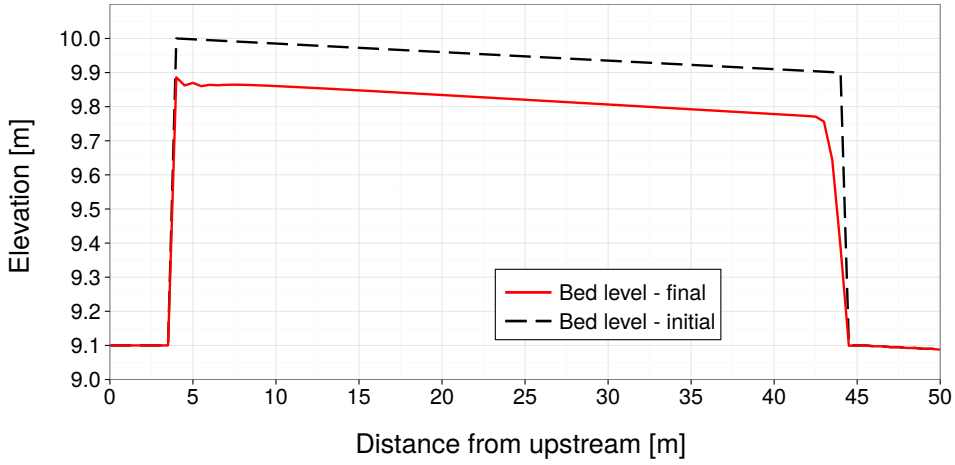

Figure 2.13 *ST_3: Guenter Test: equilibrium bed level (BC)*

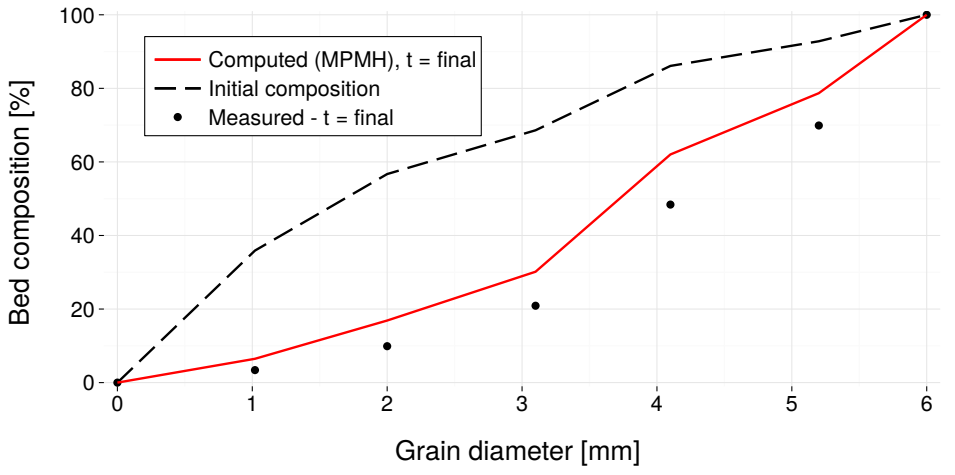

Figure 2.14 *ST_3: Guenter Test: grain size distribution (BC)*

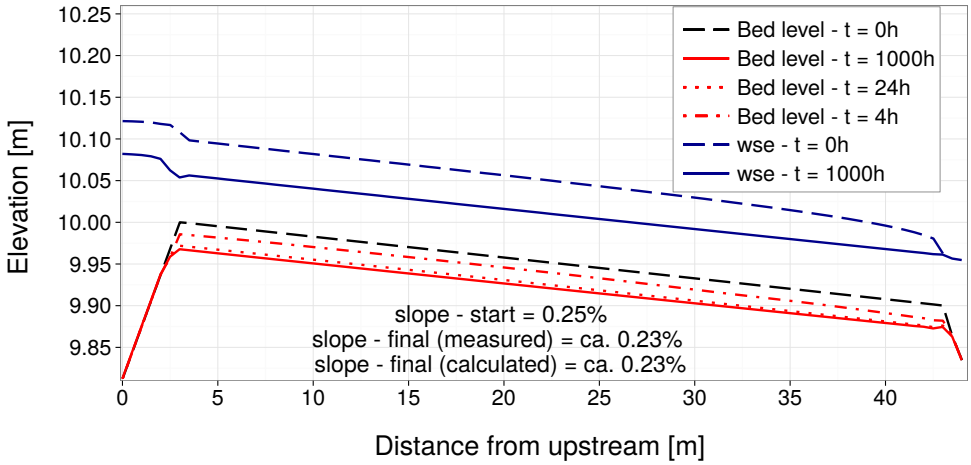

Figure 2.15 *ST_3: Guenter Test: equilibrium bed level (BP)*

the simulations and used with its default values for the pre-factor (=1.0) and the exponent of the hiding exponent (=-1.5).

The experimental flume has a mobile bed and is modelled with 312 rectangular elements. The channel parts in front and behind the experimental flume, are set to fixed bed elevations in this simulation. The sediment which leaves the mobile bed and enters the fixed bed section is removed using a sediment sink. The thickness of the bedload control volume is set to a constant value of 5 mm. The choice of the thickness of the bedload control volume shows large impacts on the simulation results. An increased thickness here results in larger erosion and a finer composition of the final bed armour.

The mobile bed is eroded during the simulation until finally an armouring layer of coarser materials is formed which prevents further erosions. The final slope of the bed is nearly constant with a value of 0.23%, which is slightly smaller than the original slope of 0.25%. This result is in agreement with the observations made by Guenter. Also the rotation of the bed surface around the downstream end of the flume can be observed during the simulation.

Figure 2.16 shows the measured and computed grain compositions, whereas the latter was taken from the upstream end of the flume. The simulated grain size distribution (red curve) shows a good qualitative agreement with the measured distribution by Guenter (blue dots). But a trend can be seen that the computed composition is slightly too fine. Finally, it can be said, that the numerical model seems capable of reproducing the sorting effects and seems able to simulate the formation of an armouring bed layer.

Beside the results obtained with the Hunziker's transport formula, Figure 2.16 presents also the resulting grain distributions obtained with Wu's transport formula (green curve). Here it can be seen that the finer fractions are eroded too strongly, but a qualitative agreement is obtained. For the simulations with the Wu formula the same critical shear stress of 0.047 was used, and the default settings of the bed load factor (=1.0) and the default exponent of the hiding-and exposure coefficient (=-0.6) were set. But to enable similar erosion volumes as obtained with the Hunziker's formula, the thickness of the bed load control volume was increased to 2.5 cm.

To check for the mass conservation properties a comparison was made between the initial

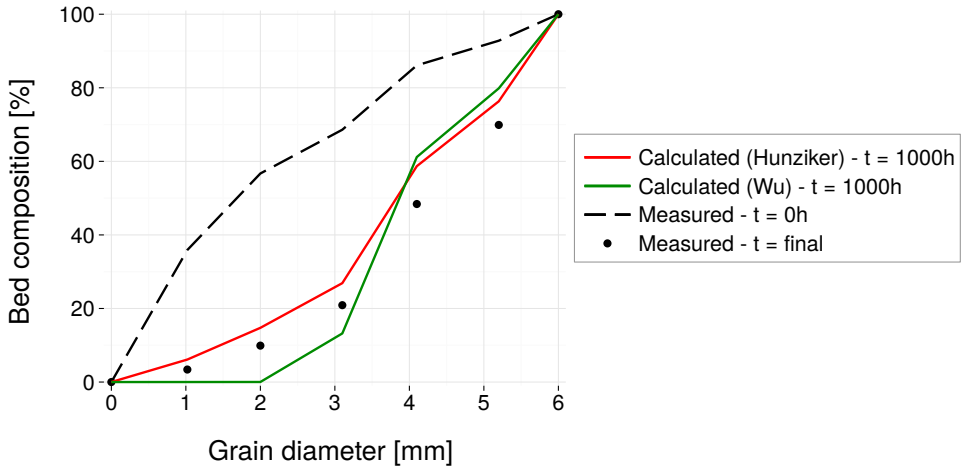

Figure 2.16 *ST_3: Guenter Test: grain size distribution (BP)*

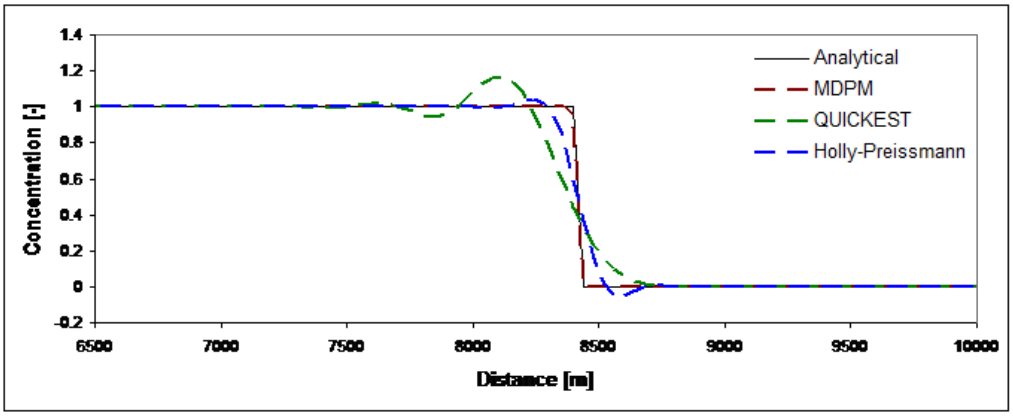

Figure 2.17 *ST_BC_1: case A, concentration after 9060 s*

sediment volumes in the flume and the final sediment volumes, under regard of all removed sediment volumes. Despite the long run time, the simulation proves to be conservative regarding the sediment transport. Since the experiment has a constant inflow rate and quasi-steady flow conditions, the 'hydro_step' approach can be used here which allows a reduction of several orders of magnitude in simulation time.

2.5.2 BASEchain specific Test Cases

2.5.2.1 ST_BC_1: Advection of suspended load

The advection test has been executed for the QUICK, the QUICKEST, the Holly-Preissmann and the MDPM-scheme. The results of the QUICK-scheme are not illustrated as they are very instable.

Case A: Figure 2.17 shows the concentration front after 9060 s or after 8200 m of way. The results show that the big issue of the advection simulation, the numerical diffusion, is almost completely avoided by the MDPM scheme.

Case B: Figure 2.18 shows the concentration front after 9772.5 s or after 8843 m of way. For

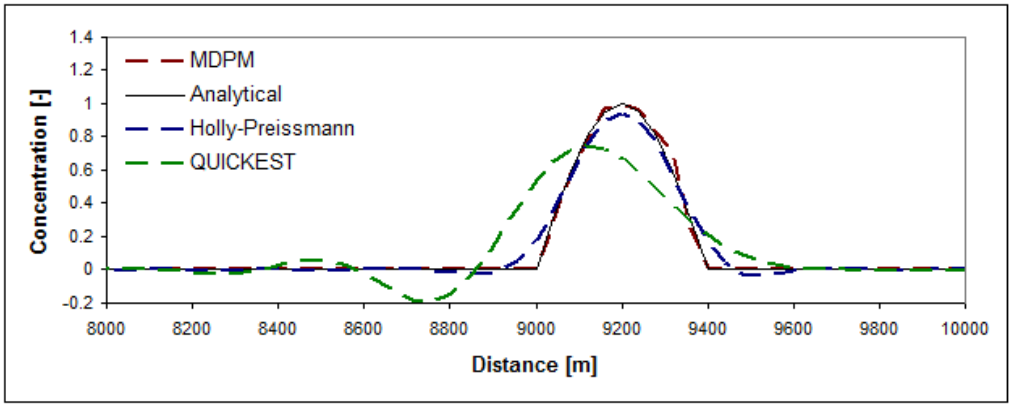

Figure 2.18 *ST_BC_1: case B, concentration after 9772.5 s*

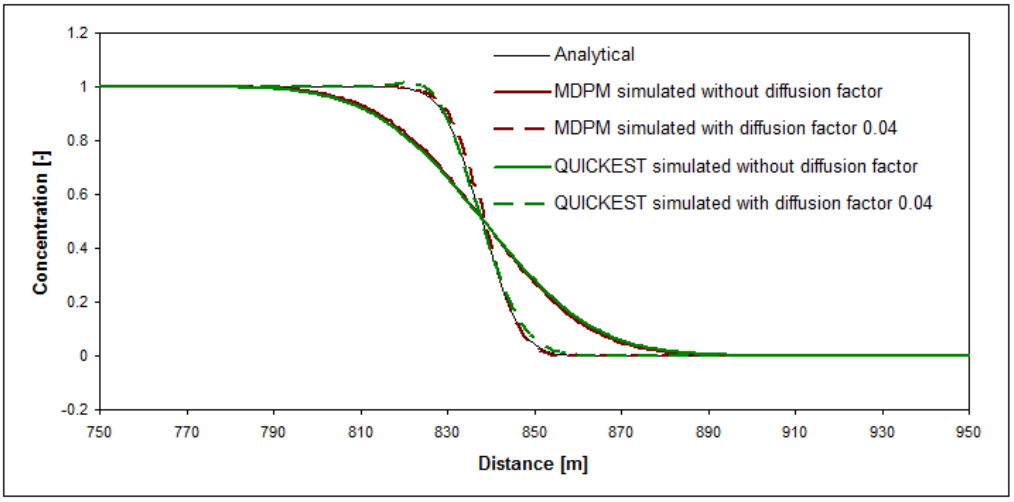

Figure 2.19 *ST_BC_2: case A, concentration after 605 s*

the MDPM scheme there are some local deviations from the analytical solution. These are due to the discretisation and do not increase with time and distance. The initial maximal concentration is conserved.

2.5.2.2 ST_BC_2: Advection-Diffusion

The Advection Test has been executed for the QUICKEST, and the MDPM-scheme. Figure 2.19 and Figure 2.20 show the concentration front of case A and the Gauss distribution for case B after 605 s or after 788 m away. The diffusion factor is 0.04 for case A and 0.1 for case B. The result of the simulation with the internally computed diffusion is also illustrated, but there is no analytical solution to compare.

The results are satisfying. The QUICKEST scheme gives here a result which is nearly as good as the one of the MDPM scheme, but this is due to the short simulation time. Its deviation from the exact solution due to numerical diffusion increases with the time like shown in test ST_BC_1.

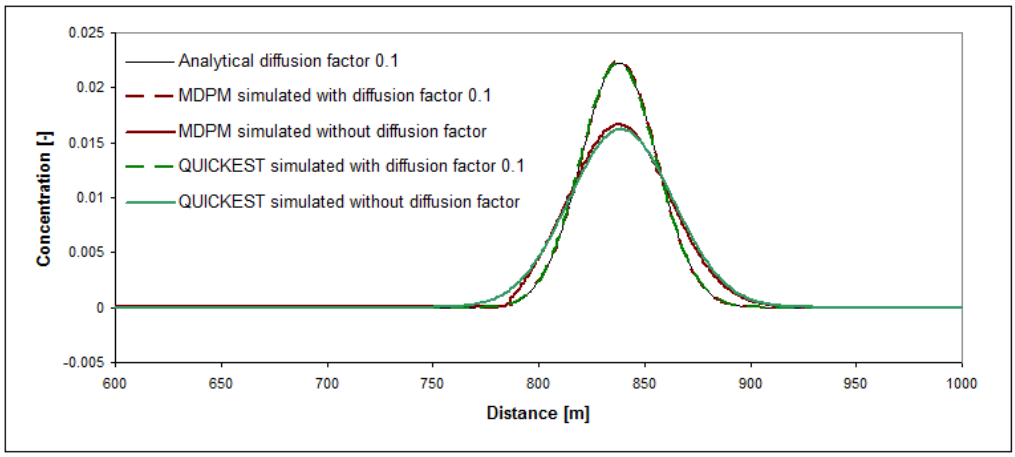

Figure 2.20 *ST_BC_2: case B, concentration after 605 s*

2.5.3 BASEplane specific Test Cases

2.5.3.1 ST_BP_1: Advection of suspended load

To test the advection of suspended sediment transport, the MDPM-scheme has been applied.

Case A: Figure 2.21 shows the concentration front after 200 s or after 730 m of distance travelled. The results show that there is no oscillation before and after the front. The diffusion is small and manly due to the irregular discretisation.

Case B: Figure 2.22 shows the concentration front after 200 s or after 700 m of distance travelled. The maximum of the Gauss distribution is conserved and there are no oscillations near the steep gradients.

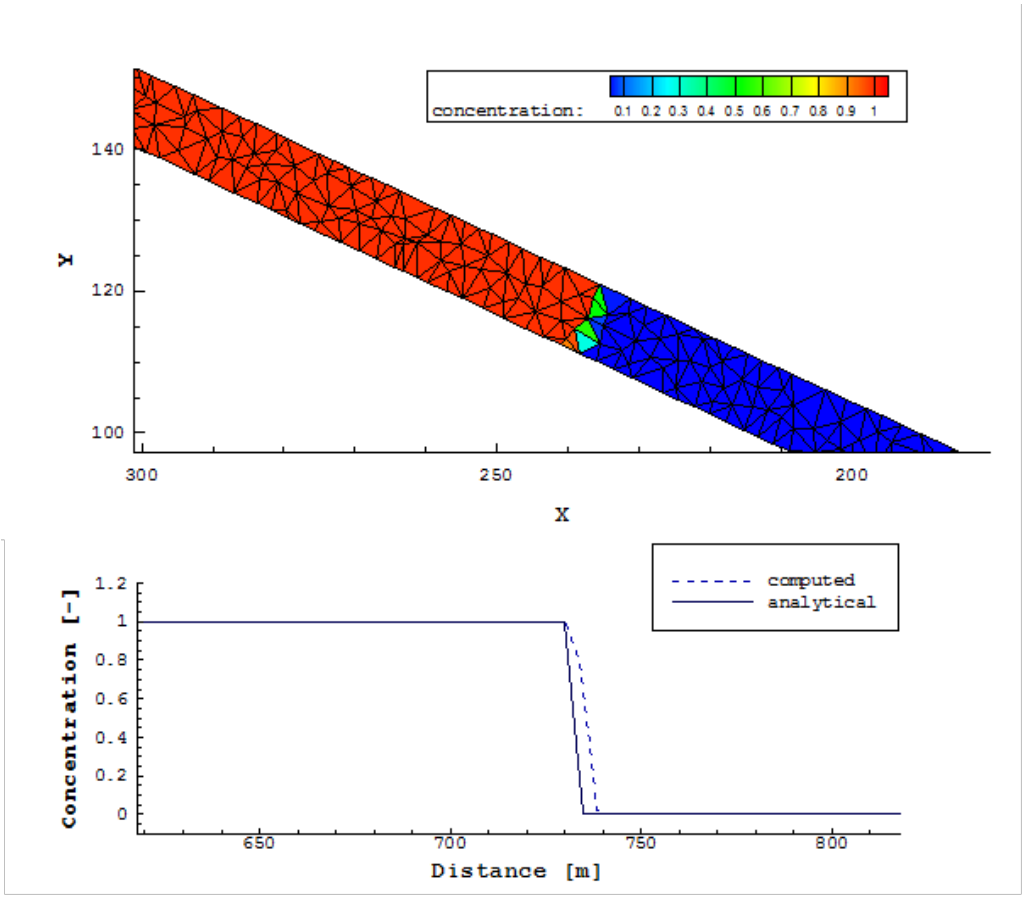

Figure 2.21 *ST_BC_1: case A, concentration after 200 s*

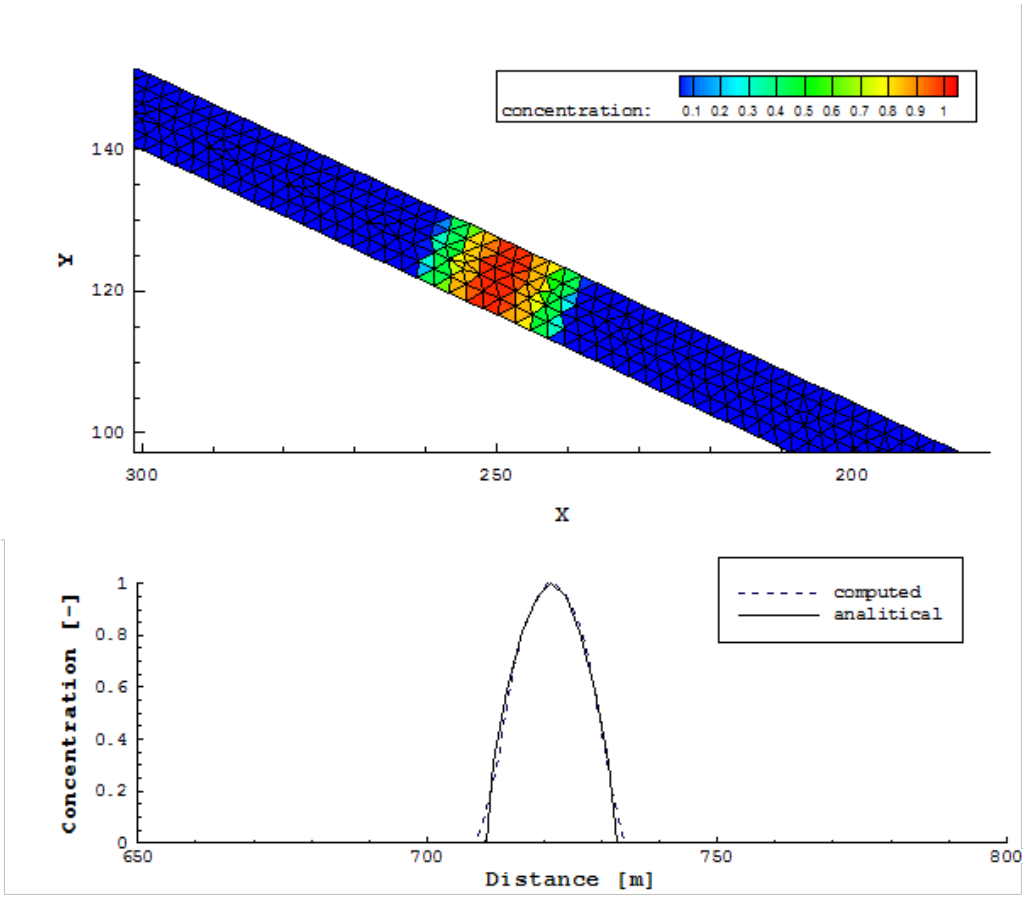

Figure 2.22 *ST_BP_1: case B, concentration after 200 s*

3

Model Coupling

3.1 Coupling of Domains of Same Type

3.1.1 COUPL_1: Sequential two-way coupling with backwater effects

3.1.1.1 Intention

This test is intended to verify and test the coupling mechanism of a sequential coupling with mutual data exchange between the sub-domains.

3.1.1.2 Description

Two sub-domains are simulated in a combined simulation. Sub-domain A is situated upstream of sub-domain B (Figure 3.1). Both sub-domains are coupled using a two-way coupling mechanism via an outflow hydrograph boundary and an inflow hydrograph boundary. Discharges are passed to the downstream sub-domain and water surface elevations are passed in upstream direction. Backwater effects travel in direction of the upstream sub-domain, caused by an outflow weir at the downstream end.

3.1.1.3 Geometry and initial conditions

- Case A: 1-D → 1-D coupling

  Both channels have trapezoidal cross sections and 1 km length, 40 m base width and a slope of 1.25 ‰.

- Case B: 2-D → 2-D coupling

  Both channels have rectangular cross sections, 1 km length, 40m width and a slope of 1.25 ‰.

- Initially the sub-domains are dry.

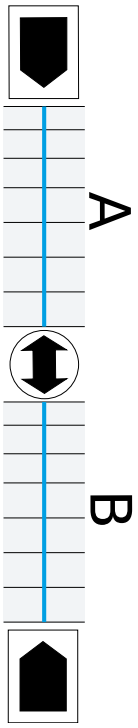

Figure 3.1 *Sub-domains A and B*

3.1.2 COUPL_2: River network modelling

3.1.2.1 Intention

This test is intended to verify and test the coupling mechanism of a junction and a bifurcation in a simple river network configuration.

3.1.2.2 Description

Five sub-domains are simulated in a combined simulation (Figure 3.2). Sub-domains A and D are situated upstream and have an inflow hydrograph defined. Both river branches merge together into the sub-domain B. At its downstream end sub-domain B splits up into sub-domains E and C. The junction and the bifurcation are simulated with one-way couplings, i.e. the upstream sub-domains are not influenced by the water elevations in the downstream sub-domains.

3.1.2.3 Geometry and initial conditions

- All channels have trapezoidal cross sections, 1 km length, 40 m base width and a slope of 1.25 ‰.
- Initially all sub-domains are dry.

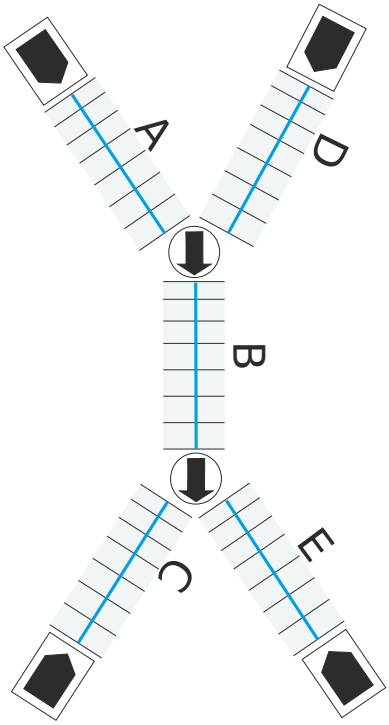

Figure 3.2 *Five sub-domains*

3.1.3 COUPL_3: Sequential coupling with sediment transport

3.1.3.1 Intention

This test is intended to verify and test the coupling mechanism of a sequential coupling in a morphological simulation with bed load and suspended load transport.

3.1.3.2 Description

Sub-domain A is situated upstream of sub-domain B (Figure 3.1). Both sub-domains are coupled using a 1-way coupling mechanism via an outflow hq-relation boundary and an inflow hydrograph boundary. Both sub-domains simulate single grain bed load transport. The bed load and suspended load are exchanged over the sequential coupling using corresponding outflow and inflow boundary conditions. At the upstream end of sub-domain A discharge, bed load and suspended load enter with constant rates.

3.1.3.3 Geometry and initial conditions

- Both channels have trapezoidal cross sections and 1 km length, 40 m base width and a slope of 1.25 ‰.
- The initial conditions for the hydraulics are uniform flow conditions in both sub-domains.
- The initial conditions for the bed load transport are set to equilibrium conditions (using IODown and IOup boundary conditions).

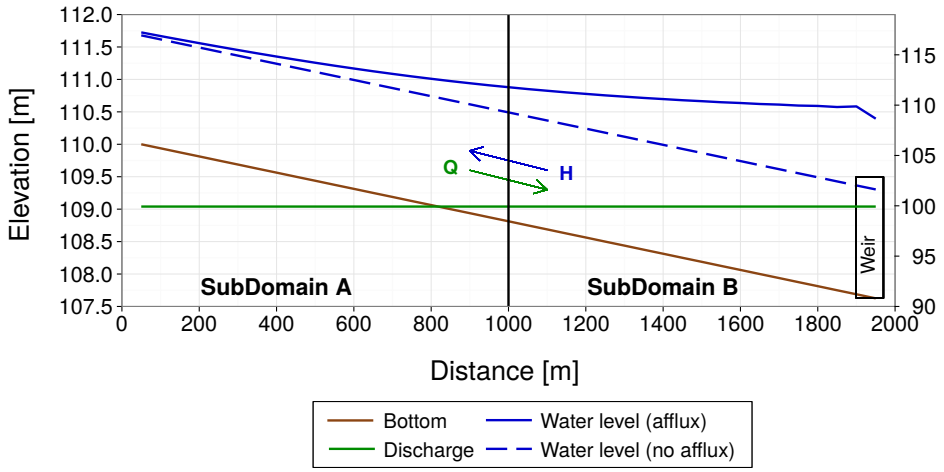

Figure 3.3 *COUPL_1_BC: Water surface elevation and discharge profiles of coupled BASEchain sub-domains A and B*

- The initial condition for the suspended sediment transport is set to concentration 0.0.

3.2 Results

3.2.1 Coupling Test Cases for Domains of Same Type

3.2.1.1 COUPL_1: Sequential two-way coupling with backwater effects

3.2.1.1.1 COUPL_1_BC: Results obtained by BASEchain

The coupling test case has been simulated starting from dry conditions in sub-domains A and B. Discharge is passed into downstream direction and water surface elevations are passed into upstream direction (two-way coupling).

After some time steady state conditions are reached in the coupled simulation. The backwater curve travels seamlessly from the downstream sub-domain into the upstream sub-domain. The discharge is constant over the whole domain. This indicates a correct two-way coupling which is capable to consider backwater effects from downstream.

3.2.1.1.2 COUPL_1_BP: Results obtained by BASEplane

As in the 1-D case, this coupling test case has been simulated starting from dry conditions in sub-domains A and B. Discharge is passed in downstream direction and water surface elevations are passed in upstream direction (two-way coupling).

After some time steady state conditions are reached in the coupled simulation. The backwater curve again enters seamlessly the upstream sub-domain. The velocity has no jumps at the interface between the sub-domains and it reduces in direction of the downstream weir.

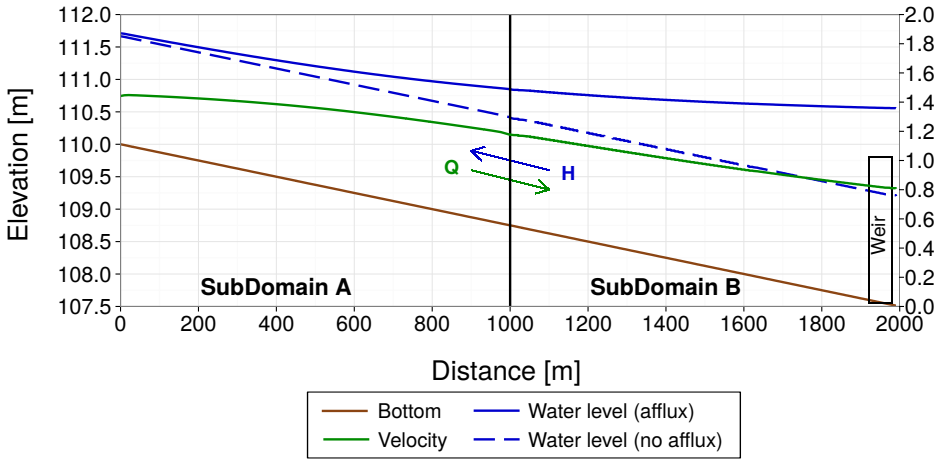

Figure 3.4 *COUPL_1_BP: Water surface elevation and discharge profiles of coupled BASEplane sub-domains A and B*

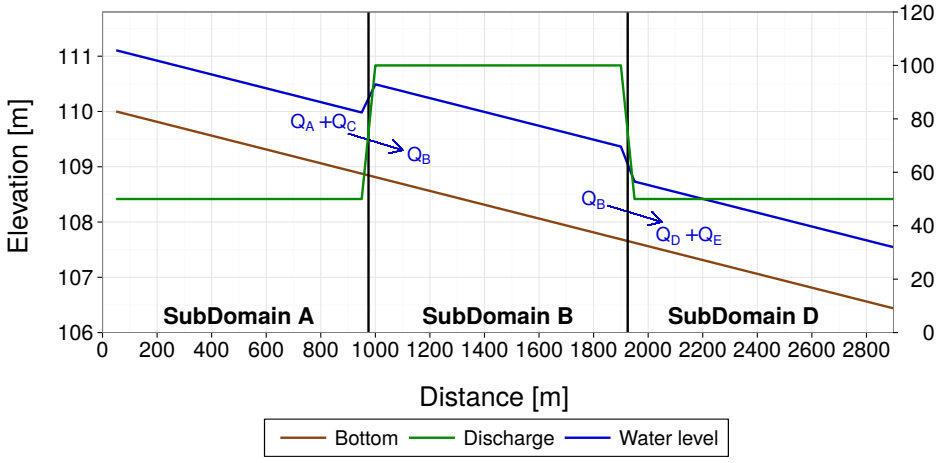

Figure 3.5 *COUPL_2: Water surface elevation and discharge profiles in the coupled river network*

3.2.1.2 COUPL_2: River network modelling

This test case has been simulated starting from dry conditions in all sub-domains. Sub-domains A and C have inflow hydrographs defined and sub-domains D and E have uniform outflow conditions defined. The discharge is passed in downstream direction using a one-way coupling, i.e. influences of downstream water levels are neglected here.

Figure 3.5 shows steady state conditions reached in the coupled simulation. The discharges leaving sub-domains A and C flow together at a junction and pass their discharge into sub-domain B. Sub-domain B splits up into two downstream sub-domains D and E (Figure 3.2). The mass conservation is fulfilled in this simulation and the discharges are distributed correctly among the sub-domains. The water levels show jumps at the coupling interfaces because their influence on the upstream sub-domains was neglected here.

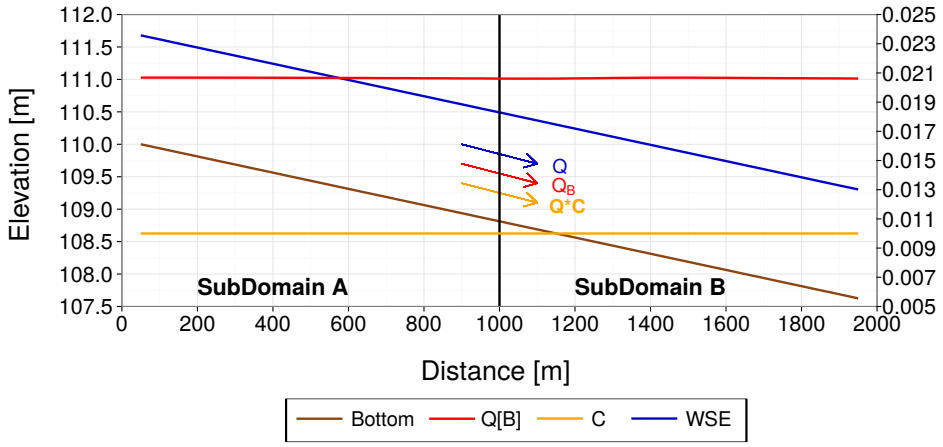

Figure 3.6 *COUPL_3: Bed load transport rate and concentration profile of coupled BASEchain sub-domains A and B*

3.2.1.3 COUPL_3: Sequential coupling with sediment transport

The sub-domains have been simulated starting from uniform flow conditions. Discharge, transported bed load and suspended loads are passed from the upstream sub-domain into downstream direction via boundary conditions. Inflowing discharge and inflow concentration profiles are constant over time. The bed load inflow is set in a way that equilibrium transport is achieved.

The simulation is run until steady state conditions are reached. As can be seen in Figure 3.6, the bed load transport rate is nearly constant in both sub-domains. Also the concentration profiles are the same in the upstream and downstream sub-domains and equal the input concentration profile.

4

Subsurface Flow

4.1 BASEsub1: Saturated, confined water flow in soil

As a first test case a steady-state subsurface flow on a mesh of 1x0.1x1 m extension is selected with a cell size of $\Delta x = 0.01$ m. The soil's hydraulic conductivity is set to $k_f = 0.001$ m/s in the computational domain.

At the west boundary a hydrostatic pressure head of $h_w = 5$ m is set as boundary condition. At the east boundary a hydrostatic pressure head of $h_e = 2$ m is set. The other boundary cells are treated as bounce-back boundaries. The numerical constant ϑ is set to 3 and the time step size is selected as Δt= 1 s. This configuration results in a confined subsurface flow with constant pressure gradient of $\partial h/\partial x = 3$.

The obtained results are illustrated in Figure 4.1, for a cross sectional cut along the y-axis through the domain. The model is able to reproduce the analytical linear gradient of the pore-water pressure head within the domain.

4.2 BASEsub2: Water infiltration into partially-saturated soil

To test the flow in the partially-saturated zone, the unsteady downward propagation of an infiltration front is simulated. This test case was chosen as described by Vogel et al. (2001), in order to allow for comparison with their results obtained with a FE-model. The same test was also successfully modelled with a LBM-approach by Ginzburg et al. (2004).

The domain is discretized with 1x0.1x1 m extension. The cell size is set to $\Delta x = 0.01$ m. As retention model the approach after Van-Genuchten and Mualem (VGM) is applied. The soil parameters are chosen as α= 0.8 1/m and $n_\nu = 1.09$ based on the tabulated values given in Vogel et al. (2001). The hydraulic conductivity is set to k_f = 5.55E–7 m/s. A negative hydrostatic pore-water pressure distribution (= soil suction) is set as initial condition with a total head of $h_w + z$ = –10 m. At the top of the domain a constant infiltration source

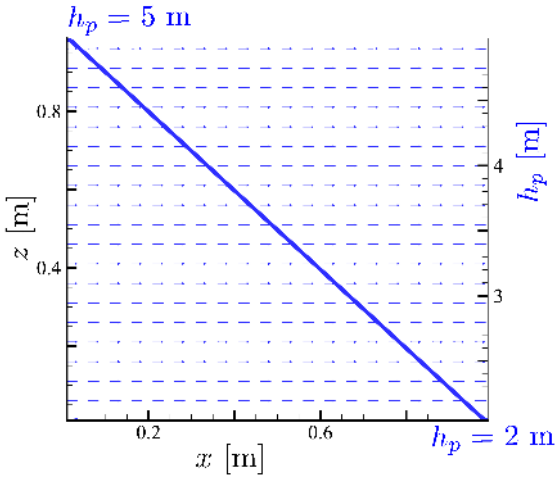

Figure 4.1 *BASEsub1: Saturated confined flow through homogenous domain with linear pore-water pressure gradient.*

is placed with q_{inf} = 2.78E–7 m/s, leading to the formation of an infiltration front. The moisture-formulation is used with $\vartheta = 3$ and a time step size of $\Delta t = 10$ s is selected.

The temporal evolution of the infiltration front was simulated with the air-entry pressure head h_s= -1E7 m. The propagation of the infiltration front through is depicted in Figure 4.2 and Figure 4.3. The propagation of the infiltration front obtained with BASEsub (left) is compared with the results obtained with the FE-model by Vogel (right), indicating only negligible deviations. The results also confirm the previously obtained results by Ginzburg.

4.3 BASEsub3: Unsaturated seepage flow

In this setup the 3-D unsteady seepage flow through a laboratory dam is modelled. The experimental investigations were made at the TU Berlin (see Pham Van (2009) for details). The homogeneous dam is 0.6 m high, 4.0 m long and 0.4 m wide. The sand dam material has a hydraulic conductivity of k_f = 9.5E-4 m/s (the value given in the reference of 0.95E-4 m/s is supposed to be a typo). The saturation moisture content of $\theta_s = 0.49$ and a residual water content of $\theta_R = 0.01$ were measured in the laboratory.

The dam is discretized with cubic cells and a cell size $\Delta x = 0.01$ m. As initial condition the measured water content of $\theta_0 = 0.115$ is applied within the whole dam. The air entry pressure is set to h_s = -0.035 m. At the upstream embankment slope a time dependent pressure boundary is applied, simulating the rising water level in the reservoir left to the dam. At the downstream embankment slope a seepage boundary is set. The VGM-model is used with α = 14.5 1/m and n = 2.68 for sand material. These VGM parameters were chosen with respect to the listed values in Vogel et al. (2001) and are not based on laboratory measurements. For the simulation, the moisture-formulation of the Richard's equation is used with $\vartheta = 3$ and a time step size of $\Delta t = 0.25$ s is selected.

Measured and simulated results of the seepage line are depicted in Figure 4.4 . The temporal development of the seepage line is in accordance between measurement and simulation throughout time.

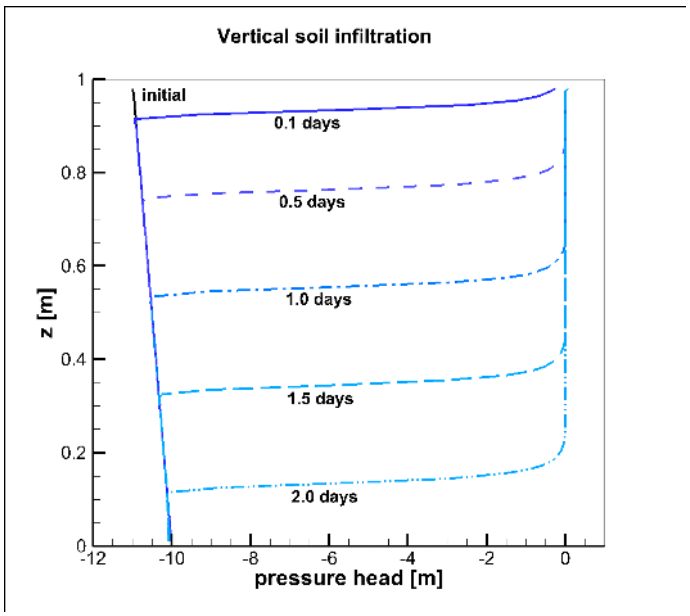

Figure 4.2 *BASEsub2: Downward propagation of infiltration front into partially-saturated soil. Simulation results of BASEsub.*

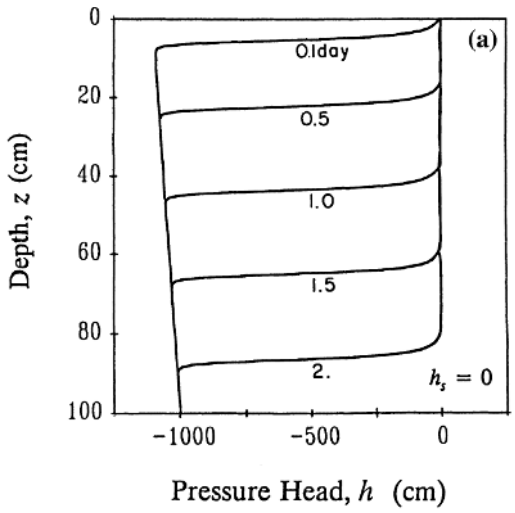

Figure 4.3 *BASEsub2: Downward propagation of infiltration front into partially-saturated soil. Results of Vogel et al.*

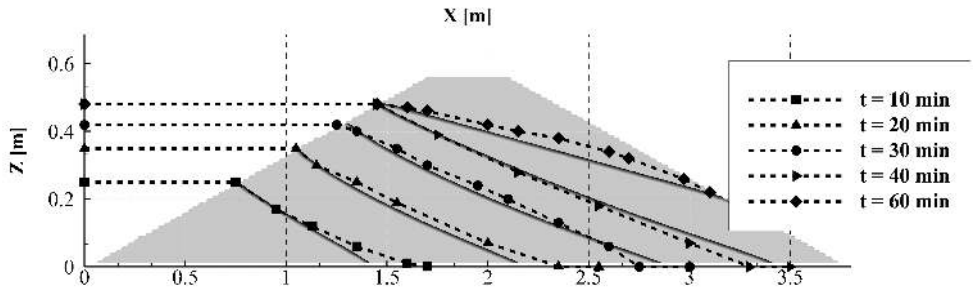

Figure 4.4 *BASEsub3: Cross sectional view of measured (dashed) and simulated (bold) development of seepage line, caused by water infiltration due to a rising reservoir at the east dam side.*

5

References

Ginzburg, I., Carlier, J. and Kao, C. (2004). Lattice Boltzmann approach to Richard's equation. *Proceedings of the CMWR XV, CT Miller*, 583–597. Chapel Hill, NC, USA.

Kassem, A.A. and Chaudhry, M.H. (1998). Comparison of Coupled and Semicoupled Numerical Models for Alluvial Channels. *Journal of Hydraulic Engineering-Asce*, 124(8): 794–802.

Pham Van, S. (2009). Application of Different Model Concepts for Simulation of Two-Phase Flow Processes in Porous Media with Fault Zones [PhD thesis]: Book Series of Institute of Civil Engineering, Volume 3, Technische Universität Berlin.

Saiedi, S. (1981b). A non-dimensional coupled numerical model of alluvial flow. *International Journal of Sediment Research*, 9(2): 59–79.

Saiedi, S. (1981a). Experience in design of a laboratory flume for sediment studies. *International Journal of Sediment Research*, 8(3): 89–101.

Soni, J.P. (1981). Laboratory Study of Aggradation in Alluvial Channels. *Journal of Hydrology*, 49(1-2): 87–106.

Soni, J.P., Garde, R.J. and Ranga Raju, K.G. (1980). Aggradation in Streams Due to Overloading. *Journal of the Hydraulics Division-Asce*, 106(1): 117–132.

Soulis, J.V. (2002). A fully coupled numerical technique for 2-D bed morphology calculations. *International Journal for Numerical Methods in Fluids*, 38(1): 71–98.

Toro, E.F. (2001). Shock-Capturing Methods for Free-Surface Shallow Flows. *John Wiley*, Chichester, New York.

Tseng, M.-H. (1999). Verification of 1-D Transcritical Flow Model in Channels. *Natl. Sci. Counc. ROC(A)*, 23(5): 654–664.

Valiani, A., Caleffi, V. and Zanni, A. (2002). Case Study: Malpasset Dam-Break Simulation using a Two-Dimensional Finite Volume Method. *Journal of Hydraulic Engineering*, 128(5): 460–472.

Vasquez, J.A., Steffler, P.M. and Millar, R.G. (2005). River 2D Morphology, Part I: Straight Alluvial Channels. *17th canadian hydrotechnical conference*, Edmonton, Alberta.

Vogel, T., van Genuchten, M.T. and Cislerova, M. (2001). Effect of the shape of the soil hydraulic functions near saturation on variably saturated flow predictions. *Advances in Water Resources*, 24: 133–144.

Wiberg, P.L. and Smith, J.D. (1989). Model for Calculating Bed-Load Transport of Sediment. *Journal of Hydraulic Engineering-ASCE*, 115(1): 101–123.

Yoon, T. and Kang, S.-K. (2004). Finite Volume Model for Two-Dimensional Shallow Water Flows on Unstructured Grids. *Journal of Hydraulic Engineering*, 130(7): 678–688.